REPORT DOCUMENTATION PAGE

Form Approved
OMB No. 0704-0188

1. REPORT DATE *(DD-MM-YYYY)*	2. REPORT TYPE	3. DATES COVERED *(From - To)*
05/11/2015	Final	16-12-2011 - 31-12-2014

4. TITLE AND SUBTITLE
Pulse Power Hybrid Energy Storage Module Development Program

5a. CONTRACT NUMBER

5b. GRANT NUMBER
N00014-12-1-0289

5c. PROGRAM ELEMENT NUMBER

6. AUTHOR(S)
Herbst, John; Hebner, Robert E.; and Gattozzi, Angelo

5d. PROJECT NUMBER

5e. TASK NUMBER

5f. WORK UNIT NUMBER

7. PERFORMING ORGANIZATION NAME(S) AND ADDRESS(ES)
The University of Texas at Austin
Center for Electromechanics
10100 Burnet Road, Bld 133
Austin, TX 78758-4497

8. PERFORMING ORGANIZATION REPORT NUMBER

9. SPONSORING/MONITORING AGENCY NAME(S) AND ADDRESS(ES)
Office of Naval Research
875 North Randolph Street
Arlington, VA 22203-1995

10. SPONSOR/MONITOR'S ACRONYM(S)
ONR

11. SPONSOR/MONITOR'S REPORT NUMBER(S)

12. DISTRIBUTION/AVAILABILITY STATEMENT
Approved for Public Release; distribution is Unlimited

13. SUPPLEMENTARY NOTES

14. ABSTRACT

15. SUBJECT TERMS

16. SECURITY CLASSIFICATION OF:			17. LIMITATION OF ABSTRACT	18. NUMBER OF PAGES	19a. NAME OF RESPONSIBLE PERSON
a. REPORT	b. ABSTRACT	c. THIS PAGE			19b. TELEPHONE NUMBER *(Include area code)*
U	U	U	UU		

Pulse Power Hybrid Energy Storage Module Development Program

Contract Number: N00014-12-1-0289
Final Report

Submitted to:

Mr. Don Hoffman
Office of Naval Research

Prepared by:

Center for Electromechanics
The University of Texas at Austin
PRC, Mail Code R7000
Austin, TX 78712
(512) 471-4496 (512) 471-0781 fax

RF 363

For further information, please contact
John Herbst
j.herbst@cem.utexas.edu

May 2015

TABLE OF CONTENTS

LIST OF FIGURES

LIST OF TABLES

1 Executive Summary

The Pulse Power Hybrid Energy Storage Module Development Program compared two systems to power large pulsed loads. The notional load used in the comparison was a high energy, capacitor-based, Pulse Forming Network (PFN) operated with a repetition rate of 12 charge/discharge cycles per minute. Two hybrid solutions were evaluated. One was based on lithium ion batteries and used a flywheel to improve the power delivery. The other was a rotating-machine based Hybrid Energy Storage Module (HESM) designed to mitigate the impact of transient (pulsed) loads on the ship's distribution power system. An important finding was that the transient load could be effectively buffered with only the flywheel energy storage element.

Two PFN charging profiles were evaluated: constant current and constant current/constant power. The constant current profile was determined to be the more efficient method for charging capacitors bur requires a peak charging power of twice the average power. Hybrid constant current/constant power charging is the recommended profile because it provides high efficiency but reduces the peak power demands on the charging power supplies and energy storage sub-system.

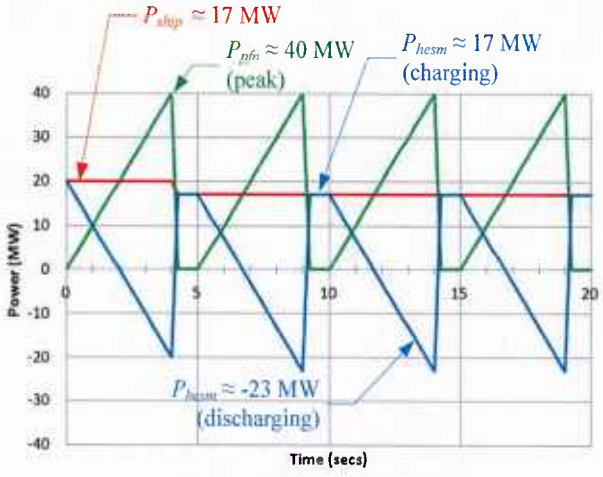

Constant Current Charging

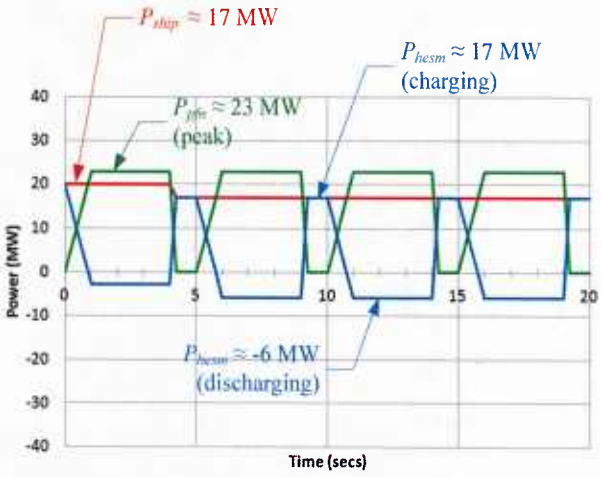

Constant Current / Constant Power Charging

Two topologies for the HESM placement within the ship's power system were considered: centralized placement of a single HESM co-located with the PFN and distributed architectures with multiple HESMs placed in different zones of the power distribution system. Each topology was evaluated using both of the PFN charging profiles. The PFN charging profiles are simulated first using controlled ideal sources for the HESM and the PFN. The ideal results showed that the approach was sufficiently appealing that more detailed assessments were warranted. The "actual" assessments used more detailed models for the power electronic converters, generators and motors used within the HESM and the ship's power system.

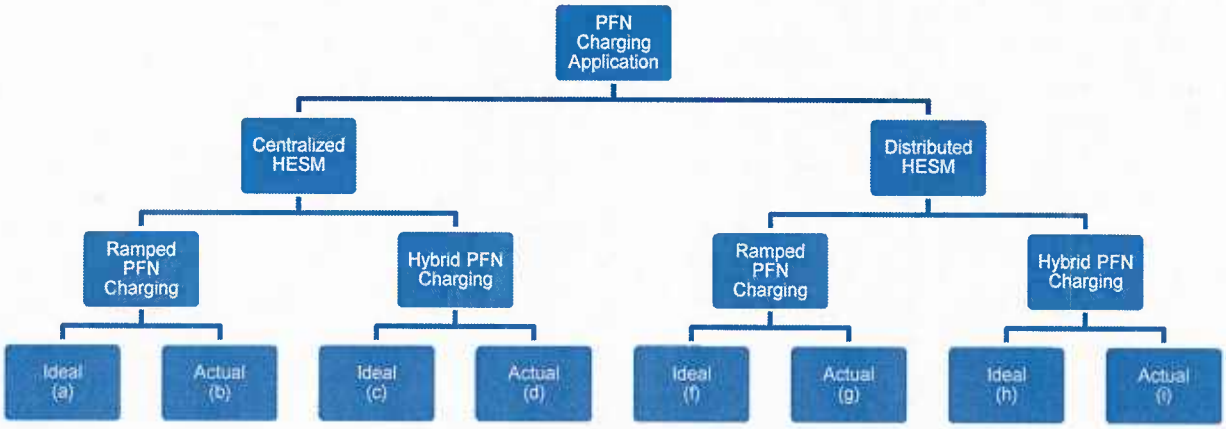

Organization of the HESM Study

Control of the HESM was accomplished by means of derived voltage reference signals that served to control the power flow in and out of the HESM controller and to maintain constant ship current. The simulation results validated this as an effective approach for control of the HESM's bi-directional converter.

The flywheel power and energy requirements closely match the characteristics of an advanced pulsed power supply developed under the Combat Hybrid Power Supply program (CHPS). A reassessment of this topology showed that it should meet the electrical requirements and the size requirements with some modification of the earlier design that was optimized for somewhat different requirements. Development and integration studies for a customized Navy variant of the concept -- the CHPS-N machine -- are being conducted under a separate ONR grant (ONR Grant N00014-14-1-0262).

The work performed showed that an architecture based on the HESM concept to minimize the impact of pulsed power loads on a ship's power system is very effective. Furthermore it confirms that the HESM can be used as an additional support element for the ship's power system when not needed for pulsed load charging (e.g. UPS duty), thus making it a versatile component for a variety of tasks.

2 Background

Future pulsed weapon and sensors will create challenges to Navy shipboard power systems [1, 2] as transient loads will constitute a significant fraction of the installed capacity. The goal of this research program is to explore the design and integration of a Hybrid Energy Storage Module (HESM) that can work to mitigate the impact of transient (pulsed) loads on the ship's power distribution system.

The evaluation has been conducted in the context of a high-energy capacitor-based Pulse Forming Network load (PFN) operated with a repetition rate of 12 charge/discharge cycles per minute. The PFN consists of multiple capacitor modules served by independent dc charging power supplies. Since this research focuses on the HESM, modeling costs were reduced by representing the PFN as a single aggregated load.

The baseline PFN charge/discharge profile requires delivering 80 MJ of energy at 80 % duty cycle with a five second repetition ratc. This translates to a 20 MW pulsed load on the ship power system for four seconds followed by a one second break to discharge the PFN (16 MW averaged over 5 seconds). (See green waveform on the left side of **Fig. 4**.) This duty cycle and load level would apply unacceptable transient loads to the ship power system. Therefore, the goal of the HESM is to provide load leveling for the pulsed PFN charging.

There are two primary options for charging of a capacitive energy store: ramped power/constant current[1] and hybrid power.[2] Constant current charging is the more efficient method for charging capacitive energy stores and is the preferred approach for capacitor charging at low power levels. In this scheme, the current into the capacitive store is constant and the power provided by the charging power supply increases linearly with capacitor voltage. This results in a ramping power profile with a peak of approximately twice the average power. For this application, constant current charging requires a peak charging power of ~40 MW and a charging system sized for this load even though it represents only a small fraction of the duty cycle.

Simulations demonstrate that the hybrid power-charging scheme requires slightly higher currents from the PFN charging power supplies, but the peak power demand on the charging power system is much lower. Furthermore, in the hybrid approach proposed herein, the charging power profile is initially ramped before it transitions to a constant power mode that reduces the peak demand on the ship power system and HESM.

---

[1]Ramped power upstream of the PFN power supply corresponds to constant capacitive-charging-current downstream of the PFN power supply.

[2] Power delivered to PFN power supply first ramps then remains constant.

3 Report Organization

This report is organized as depicted by **Fig. 1**. The research addressed two topologies for the HESM placement: centralized and distributed. Subsequently, each topology is evaluated using two PFN charging variants: ramped power and hybrid power. Each PFN charging profile is then simulated using two approaches. When using ideal sources for the HESM and PFN, the simulation type is termed *ideal* to distinguish them from the case of using a power converter and machine model to represent the HESM (termed *actual*). The assessment was initially performed with idealized components as a screening tool. The ideal results showed that the approach was sufficiently appealing that more detailed assessments were warranted. Differences between the ideal and actual simulations approaches are discussed as they are presented.

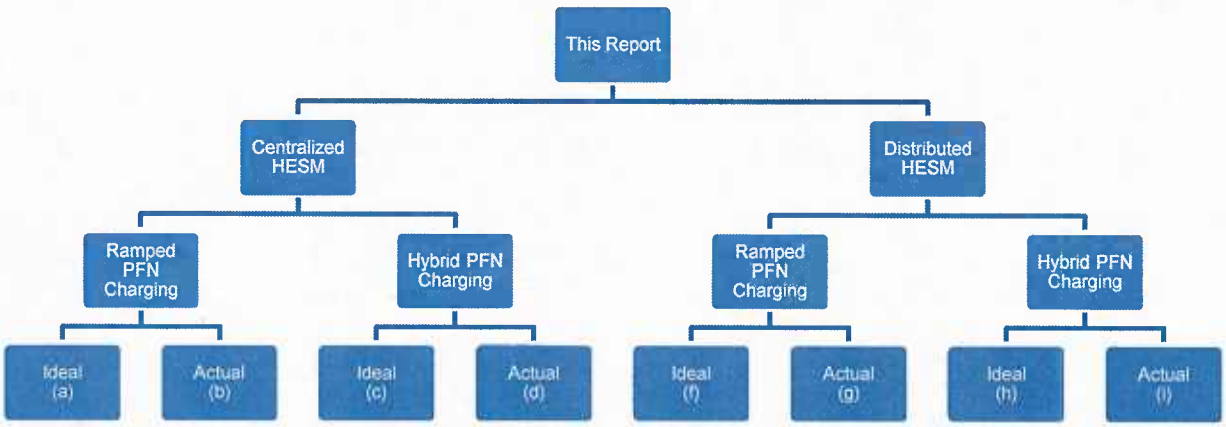

Fig. 1. Organizational chart outlining information contained in this report. *Level* 1: HESM placement (centralized vs. distributed); *Level* 2: charging mode (ramped vs. hybrid); *Level* 3: simulation type (ideal or actual). Case studies presented herein are labeled (a) through (i).

The bottom row in **Fig. 1** shows letters to indicate that this report contains eight simulation result sets (*a* through *i*) corresponding to actual and ideal simulations of the two HESM topologies and two PFN charging profiles. For each of these baseline case studies, a medium voltage dc (MVDC) distribution system [3] was selected; alternative electric power distribution architectures would primarily impact the power conversion modules providing the interface to the HESM modules.

This remainder of this report is organized as follows.

- Section 4 introduces the HESM topologies
- Section 5 introduces the PFN charging variants
- Section 6 presents simulation results of the centralized HESM topology
- Section 7 presents simulation results of the distributed HESM topology
- Section 8 provides insights on the intended machine characteristics
- Section **Error! Reference source not found.** presents interim summary and conclusions
- Section **Error! Reference source not found.** lists items currently under investigation

4 HESM Topologies

4 HESM Topologies

4.1 HESM Topology 1: Centralized

A one-line diagram [4] of the MVDC distribution architecture with a centralized HESM topology is shown in **Fig. 2**. The PFN and HESM are connected from zone 1 at an isolated dc bus. This topology implies a single dc feeder to serve both the HESM and PFN, compartmental proximity between the HESM and PFN, and the maximum storage requirement for the single HESM unit.

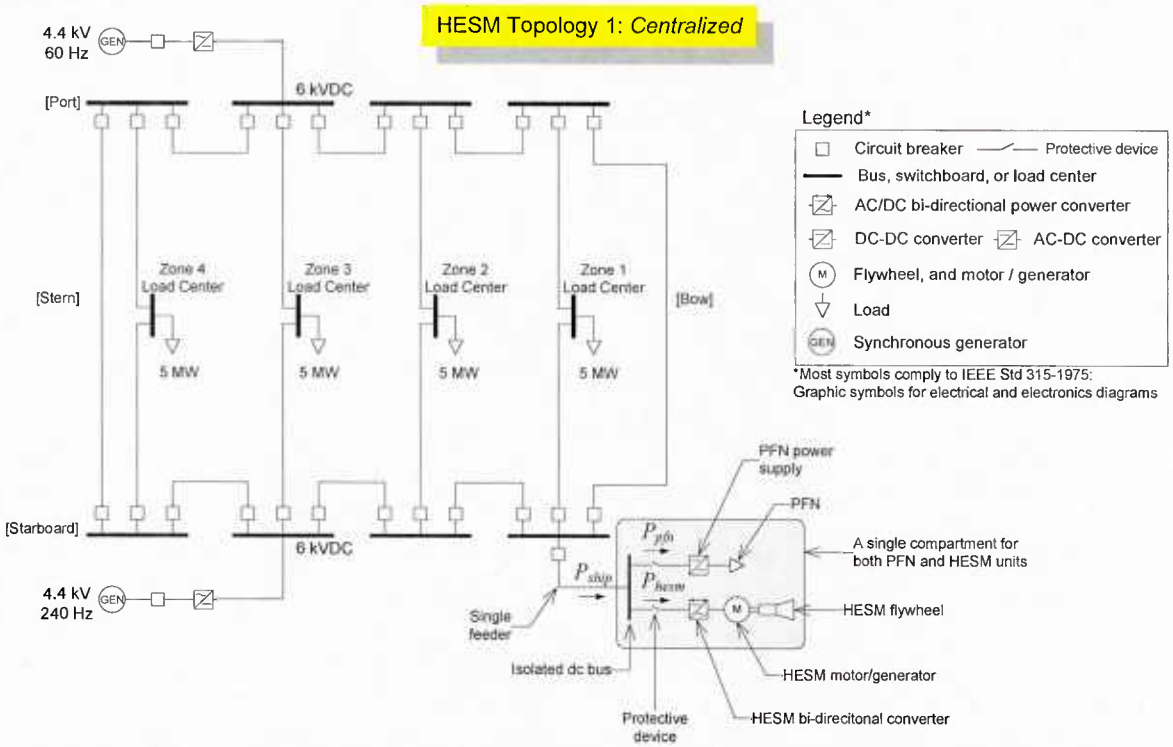

Fig. 2. MVDC architecture with a centralized HESM and PFN connected at an isolated dc bus.

4.2 HESM Topology 2: Distributed

The one-line diagram of the MVDC distribution architecture with a distributed HESM topology is shown in **Fig. 3**. The two HESM units considered for this topology are distributed over zones 2 and 3. Additional HESM modules can be considered using the same control approach developed for this initial case. The PFN remains connected to zone 1 for consistency with the centralized topology shown in **Fig. 1**. The advantages of the distributed topology are the inter-zonal placements that allow the HESMs to supplement generation ride-though when the ring bus is open, reduced failure probability under battle impact, and simplified integration. Furthermore, each distributed HESM unit is smaller and weighs less than the single HESM unit in the centralized case.

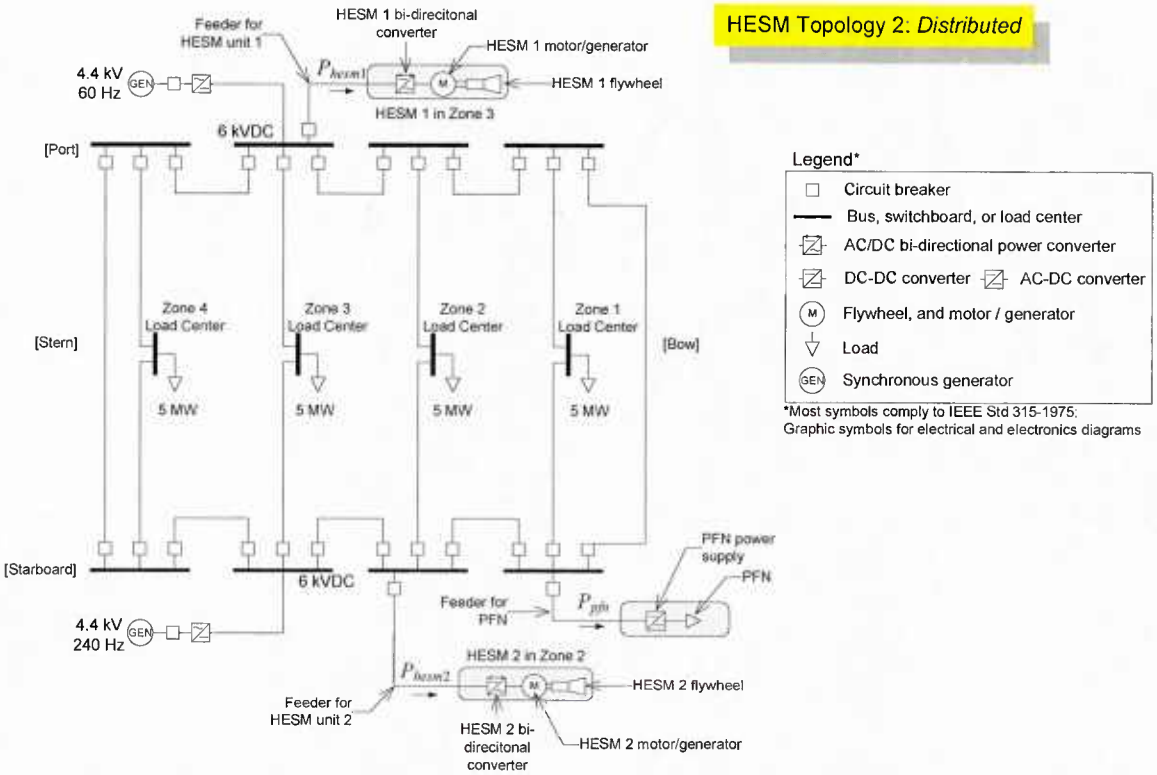

Fig. 3. MVDC architecture with distributed (zonal) HESMs and a PFN.

The assumed lengths and per-unit-length impedances for the relevant shipboard cables and feeders used in the simulation models are listed in Table 1. As a first approximation, conductor types, ampacities, voltage regulation, material characteristics, flexibility, geometric shape, economics, operating temperature, insulation [5], standing, temperature, and number shipboard cable conductors [1, 6, 7] required to supply the necessary current levels are not considered as they have a minimal impact on the simulation results. However, conductor selection is contingent upon these considerations [8] which may be important in more detailed studies.

Table 1. Resistance of relevant cables.

Cable or feeder		Length (feet)	DC Resistance* (Ω)
From	To		
Ship ring	Isolated dc bus	16.4	133E-6
Isolated dc bus	HESM	32.8	266E-6
Isolated dc bus	PFN	32.8	266E-6
Ship ring	HESM unit 1	16.4	133E-6
Ship ring	HESM unit 2	16.4	133E-6
Port	Starboard	328	3E-3

*Calculated at 8.11 mΩ/1000 ft. at 25 °C

5 PFN Charging

In the centralized case of **Fig. 2**, the ship power (P_{ship}) is the power delivered from the ship's ring bus to the dc bus connected to it (zone 1). The objective of the HESM is to minimize transients on this parameter. The PFN power (P_{pfn}) is the power delivered directly to the PFN power supply. The HESM has two power levels associated with it: a positive/charging power and a negative/discharging power. Both of these power levels are denoted as P_{hesm} and vary only in their direction (positive to mean charging or negative to mean discharging). The HESM *charging* power ($P_{hesm}>0$) is the power delivered from the isolated dc bus to the HESM bi-directional converter as shown in **Fig. 2**. This power flows through the bi-directional converter and motor/generator toward the flywheel. The HESM *discharging* power ($P_{hesm}<0$) is the power flowing away from the HESM bi-directional converter toward the isolated dc bus. The HESM discharge power *supplements* the ship power when the PFN charges—that is, when the PFN charges $P_{pfn}=P_{ship}-P_{hesm}$; and when the PFN idles and the HESM charges, $P_{pfn}=0$ and $P_{ship}=P_{hesm}$. Note that P_{hesm} is negative when the HESM is supplying power to the PFN.

In the distributed case of **Fig. 3**, P_{ship} is the power *contribution* of the two ship generators toward charging the HESM and/or PFN. The PFN power is the power delivered from the ship ring bus to the PFN power supply. The total HESM power (P_{hesm}) is the power delivered to or from the ring bus to the two HESM units together.[3] That is, the total HESM power is $P_{hesm}=P_{hesm1}+P_{hesm2}$. Similar to as shown in **Fig. 2**, P_{hesm} is shown in the charging direction (into the HESM).

5.1 PFN Charging Variant 1: Ramped Power/Constant Current

The first PFN charging variant considered is the ramped power/constant current. The PFN charging system can be modeled as an array of independent high-voltage charging power supplies each charging individual capacitor modules. This charging scheme is the most efficient but requires the highest peak power from the PFN charging power supplies and HESM. The baseline ship, HESM, and PFN power profiles corresponding to the ramped power charging profile are shown on the left of **Fig. 4**. The goal of the HESM is to level the PFN charging load seen by the ship power system—that is, to level P_{ship} to a near constant value. During the initial stages of the PFN charging profile where power into the PFN is low, the HESM accepts power from the ship ($P_{hesm} > 0$) indicating charging of the energy store. As the PFN power increases and reaches $P_{pfn}=P_{ship}$, the HESM power reverses to provide power ($P_{hesm}<0$) to the isolated dc bus to supplement P_{ship} during the latter stages of the PFN charging profile, which is when $P_{pfn} > P_{ship}$.

5.2 PFN Charging Variant 2: Hybrid Power

The second PFN charging variant is a hybrid power scheme that results in the power profiles shown on the right of **Fig. 4**. The PFN charges with a combination of constant capacitive-charging current (rising power edge between $t = 0$ and $t = 1$ s) and, subsequently, constant power (between $t = 1$ and $t = 4$ s).

---

[3] It is assumed that the HESM units charge and discharge in unison.

Under this second charging variant, the discharge HESM power is different. In charging variant 1, the HESM discharge power was P_{hesm}=23 MW while in variant 2 it is P_{hesm}=6 MW. The *charging* HESM power, however, in both variants is the same. The ship power in both cases is also the same for variants 1 and 2, which satisfies the aforementioned goal of ship load-leveling with an HESM. The primary advantages of charging variant 2 are reduced peak HESM power, reduced energy transfer through the HESM, and reduced peak power from the charging power supplies.

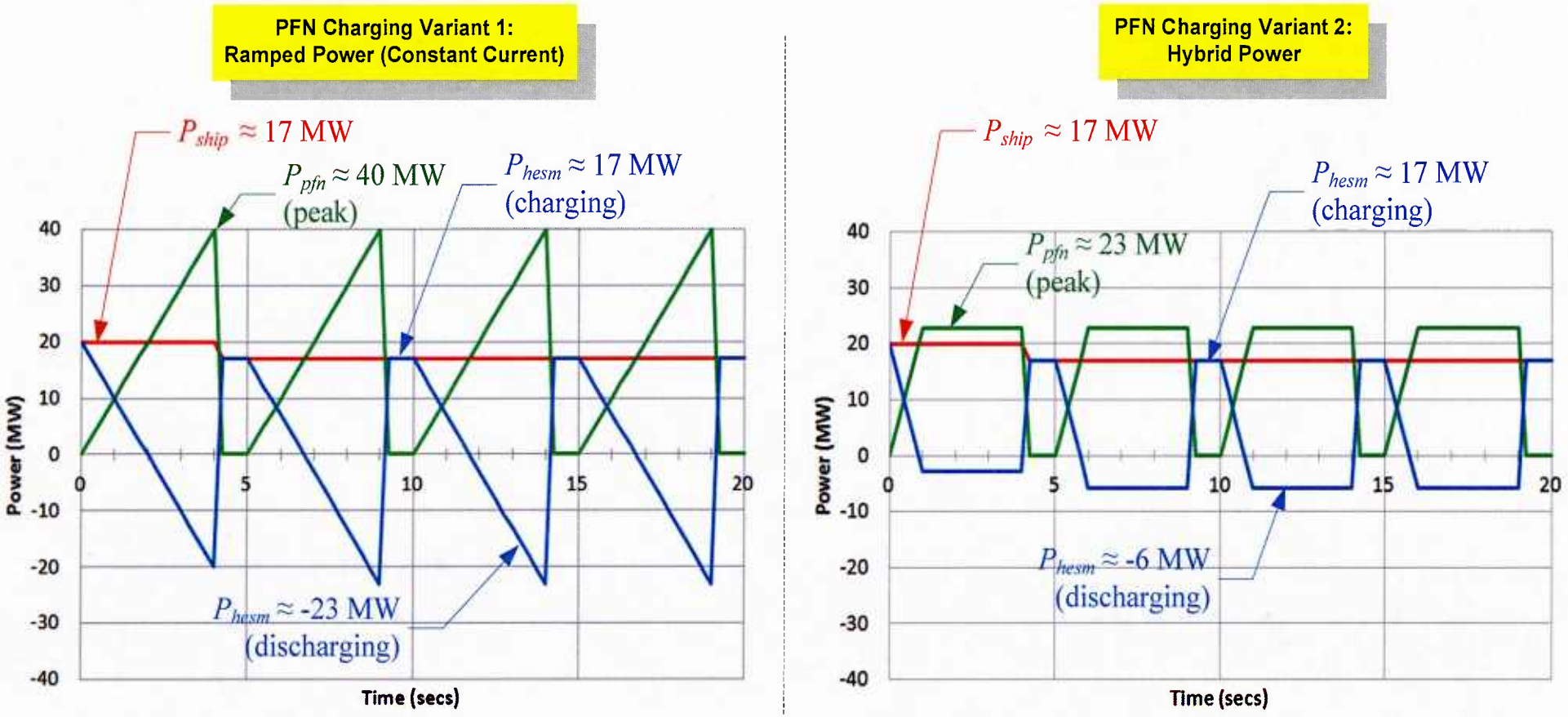

Fig. 4. Intended power profiles for the ship, PFN, and HESM for a centralized topology. Left: ramped PFN charging. Right: hybrid charging. The HESM power (blue) levels the ship power demand to 17 MW (red) during the PFN charging cycles (green).

6 Centralized HESM

This section analyses the performance of the HESM unit in the centralized topology shown in **Fig. 2**. A voltage reference signal for the HESM bi-directional converter is derived first. This voltage reference signal allows the system to charge and discharge the flywheel energy store while maintaining the ship power constant (leveled). The voltage reference signal derived next requires specifying the desired (leveled) ship current, and will be derived using an amp-hour balance. (Alternative control schemes are possible; this approach was selected to allow the study to focus on characterizing the rotating machines.)

After the derivation of the voltage control signal, the simulation results validate the HESM bi-directional converter voltage controller against the intended profiles shown on the *left* of **Fig. 4**. The simulation results include the energy stored (delivered) to (from) the flywheel, which brings about important considerations to size the HESM motor/generator.

6.1 Centralized Voltage Control

This section derives a voltage reference signal for the HESM bi-directional converter. Referring to **Fig. 2**, the sum of currents at the isolated dc bus is given by (6.1), where I_{ship} is the ship current flowing from the ring bus to the isolated dc bus, I_{hesm} is the HESM charging current, and I_{pfn} is the PFN charging current. As it is noted from **Fig. 2** and **Fig. 3**, these currents follow the directions of their respective powers.

$$I_{ship} = I_{hesm} + I_{pfn} \tag{6.1}$$

Expressing I_{hesm} in terms of the isolated dc bus voltage V_{dc} and HESM converter output voltage V_{hesm} results in (6.2), where R_{cable} is cable (feeder) resistance between the ring and isolated dc bus.

$$I_{hesm} = \frac{(V_{dc} - V_{hesm})}{R_{cable}} \tag{6.2}$$

Substituting (6.2) into (6.1) results in (6.3), where solving for the HESM converter output voltage results in (6.4).

$$I_{ship} = \frac{(V_{dc} - V_{hesm})}{R_{cable}} + I_{pfn} \tag{6.3}$$

$$V_{hesm} = \underbrace{V_{dc}}_{\substack{\text{must be} \\ \text{measured}}} - R_{cable}\left(I_{ship} - \underbrace{I_{pfn}}_{\substack{\text{must be} \\ \text{measured}}}\right) \tag{6.4}$$

Equation (6.4) is the voltage reference signal of the HESM bi-directional converter. This reference signal determines whether the HESM should charge (when $V_{dc}>V_{hesm} \rightarrow P_{hesm}>0$) or discharge (when $V_{dc}<V_{hesm} \rightarrow P_{hesm}<0$). This equation also indicates that V_{dc} and I_{pfn} must be measurable quantities and that I_{ship} is an exogenous constant, which is derived using an amp-hour balanced in section 6.2.1.

Specifying I_{ship} requires exercising care as inaccurate values result in the HESM flywheel drifting in speed. For example, if the HESM charging amp-hours are *positively* unbalanced, the HESM flywheel will continue to (slowly) accelerate indefinitely. If the HESM charging amp-hours are negatively unbalanced, the HESM flywheel will (slowly) decelerate until it stalls.

6.2 Ramped Power

This section first derives a value for I_{ship} in (6.4) using an amp-hour balance. Following, the simulation results for the HESM centralized topology with ramped power / constant current PFN charging are presented (result set (a) in **Fig. 1**).

6.2.1 Amp-Hour Balance

Referring to the HESM charging power on the left of **Fig. 4** (blue waveform), the corresponding charging current I_{hesm} over one charging cycle is depicted with **Fig. 5** . When $I_{hesm}>0$, the HESM charges; when $I_{hesm}<0$, the HESM discharges. This profile shows three time segments denoted by T_1, T_2, and T_3. During T_1, I_{hesm} (initially charging the HESM at $I_{hesm}=I_{ship}$) decays linearly from $I_{\max} = I_{ship}$ to $I_{\min} = I_{ship} - I_{pfn}^{peak}$. The ending value of I_{hesm} is negative, which means that I_{hesm} reverses direction to discharge the HESM when $I_{pfn}>I_{ship}$. During T_2, I_{hesm} reduces, reverses, and ramps back to the maximum HESM charging current of $I_{hesm}=I_{ship}$. During T_3, the HESM current is maintained at $I_{hesm}=I_{ship}$ to re-charge the HESM. This three-segment cycle repeats every 5 seconds.

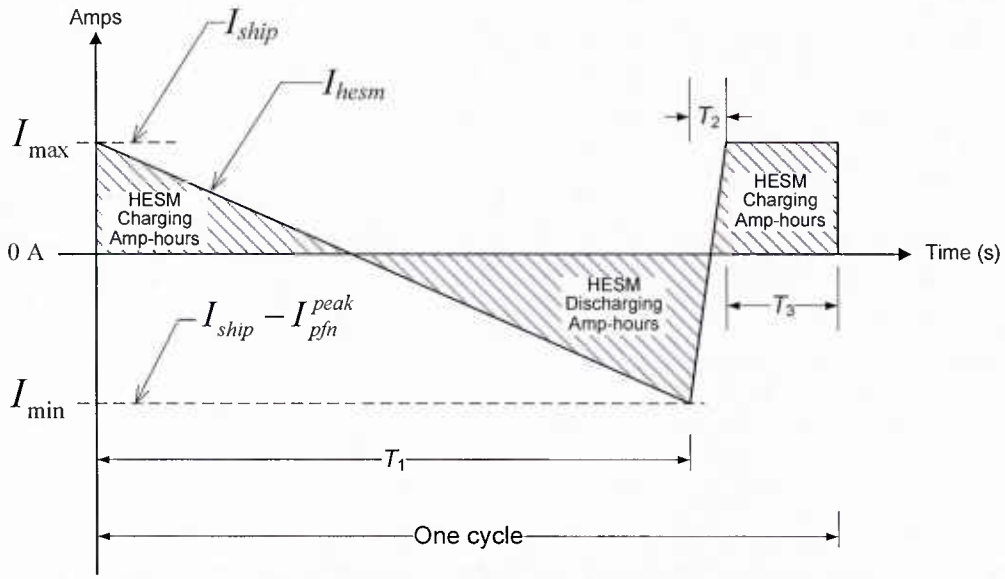

Fig. 5. Amp-hour balance for ramped power (charging variant 1).

Referring to **Fig. 5**, the desired value of $I_{max}=I_{ship}$ is approximated by balancing the shaded amp-hour areas. The net sum of amp-hours is given in (6.5), where solving for I_{ship} results in (6.6).

$$\int_{T_1}\left(\frac{I_{\min}-I_{\max}}{T_1}t + I_{ship}\right)dt + \int_{T_2}\left(\frac{I_{\max}-I_{\min}}{T_2}t + I_{\min}\right)dt + \int_{T_3}\left(I_{ship}\right)dt = 0 \tag{6.5}$$

$$I_{ship} = \frac{I_{pfn}^{peak}\left(T_1+T_2\right)}{2\left(T_1+T_2+T_3\right)} \approx 0.425 \times I_{pfn}^{peak} \tag{6.6}$$

Equation (6.6) suggests that to maintain constant ship power demand and prevent flywheel speed drifts, I_{ship} should be ~40% of the peak PFN charging current. Referring to the time periods

shown in **Fig. 2**, substituting T_1=4 s, T_2=0.25 s, T_3=0.75 s, and $I_{pfn}^{peak} = 40\ \text{MW}/6\ \text{kV} \approx 6,666\ \text{A}$ in (6.6) results in (6.7).

$$I_{ship} \approx 2,833\ \text{A} \tag{6.7}$$

The constant (leveled) value of I_{ship} in (6.7) must be maintained by the ship to prevent flywheel speed drifts. This value conforms to the expected ship power demand of $P_{ship} \approx 17$ MW on the left of **Fig. 4** and as given by (6.8).

$$P_{ship} = 2.83\ \text{kA} \times 6\ \text{kV} \approx 17\ \text{MW} \tag{6.8}$$

Having derived I_{ship} for use with the voltage reference signal of (6.4), the following subsection presents preliminary simulations results to validate (6.4) and (6.7).

6.2.2 Simulation Results

This subsection presents simulation results of the scenario in **Fig. 2** using, first, power-controlled ideal sources for the PFN and HESM units ((a) and (c) in **Fig. 1**) and, then, using a bi-directional converter, motor/generator, and flywheel for the HESM ((b) and (d) in **Fig. 1**). These two simulation run sets are termed *ideal* and *actual* in **Fig. 1**, respectively.

6.2.2.1 Simulation with Ideal Sources (a)

Referring to **Fig. 2**, the ring bus was modeled with two rectified synchronous generators serving 10 MW zonal loads. The PFN was modeled as a power-controlled current source calculated during run time as $I_{pfn} = P_{pfn}/V_{pfn}$, where P_{pfn} is known from the power profile on the left of **Fig. 4** and V_{pfn} is the voltage measured at the PFN input terminals. The HESM was modeled as a controlled voltage source driven with (6.4) and (6.7). The ideal simulation results for the centralized HESM topology, ramped power PFN charging profile are shown on the *left* of **Fig. 7** and summarized next:

Voltages: The top curve set shows dc bus, PFN, and HESM terminal voltages. These voltages are nearly the same as the voltage drop across cables of short length is negligible. Although not readily clearly visible, the HESM bi-directional converter controller ramps V_{hesm} about V_{dc} using (6.4) to produce bidirectional power flows in and out of the HESM. The PFN voltage V_{pfn} ramps down during the PFN charging periods due to the voltage drop of its feeder, and it returns to V_{dc} when the PFN idles between discharge cycles.
Current: The second curve set on the *left* of **Fig. 7** shows the PFN, HESM, and ship current. The leveled ship current is consistent with the computed value of the amp-hour balance in (6.7).

Power: The third curve set on the *left* of **Fig. 7** shows $P_{ship} \approx 17$ MW, which is consistent with the calculation in (6.8) and with the leveled ship power on the left of **Fig. 4** (red trace). The PFN charging power P_{pfn} is also in agreement with charging variant 1 anticipated by **Fig. 4**. The HESM power P_{hesm} is bi-directional: $P_{hesm}>0$ indicates the HESM is charging and $P_{hesm}<0$ indicates the HESM is discharging.

Energy: The fourth curve set on the *left* of **Fig. 7** shows the energy delivered from the ship ring bus and the energy consumed by the PFN. The energy stored in the HESM is displayed

as flywheel speed (RPM) against the right-side vertical axis. The flywheel speed was calculated from the relation of energy stored in a rotating mass as

$$W = \frac{1}{2} J \omega^2 \tag{6.9}$$

where

W = energy stored in flywheel mass [Joules]
J = flywheel moment of inertia [kg-m^2]
ω = flywheel angular speed [rad/s].

For the initial simulations, the flywheel's moment of inertia was set to J=1,128 kg-m^2, which is the same as the rotor inertia of an Electromagnetic Aircraft Launch System (EMALS) pulse power generator [9]. Expressing ω as revolutions per minute (N, RPM) results in (6.10).

$$N = \frac{60}{2\pi} \sqrt{\frac{2}{J} W} \ \text{(RPM)} \tag{6.10}$$

As noticed from the HESM speed trace (N_{hesm}) in **Fig. 7**, there is a drift in flywheel speed. This drift is due to a minor unbalance neglected in the amp-hour analysis. The balancing equations do not account for some real life issues like dc voltage ripple, the exact voltage level at the isolated dc bus, and the exact charging/discharging values of I_{hesm}. The flywheel speed drift has been in fact compensated by the addition of a speed control loop feedback on the power converter. This speed loop feedback was added in the final version of the models delivered to the Navy and has reduced the flywheel speed drift to an inconsequential level. This solution, of course, was accomplished by intervening via the software on the model design not on the foundational analytical equations described above which, in and of themselves, do not address this issue.

6.2.2.2 Simulation with Actual Sources (b)

Referring to **Fig. 2**, the two generators providing the power to the main ring bus were modeled as wound field synchronous machines with their output rectified by a 12-pulse rectifier. The field voltage of the synchronous generator was regulated to maintain a constant output voltage of 4,444 VAC (rms, line-to-line) rectified to 6 kV dc.

The HESM motor/generator was modeled as a programmable three-phase voltage source with a nominal output of 3,500 V ac (rms line-to-line) and with an inertia of 1,128 kg-m^2 (corresponding to the EMALS machine) representing the flywheel energy storage. The flywheel storage can be either the rotor of the motor/generator or a separate rotating unit coupled mechanically to it. The motor/generator is connected to the isolated dc bus via a bi-directional power converter. The converter accepts variable frequency ac power from the flywheel-generator storage and provides rectified output dc power, or accepts power from the isolated dc bus and converts it to three-phase ac power to drive the synchronous machine as a motor and store energy in the flywheel. The bi-directional converter is controlled by considering the d-q axes representation of its current and actively controlling the direct axis component [10]. The PFN load was modeled as a power-controlled current source just as was done in the ideal case.

The results of the simulations with actual sources are summarized in **Fig. 9** (left). As can be seen, they reproduce very closely the results obtained with ideal sources (**Fig. 7**) except for the

voltages. In the ideal simulations ((a) and (c)), the six-pulse generator rectifiers and absence of voltage regulation produced significant dc voltage ripple. However, this ripple was ignored because it did not affect the simulation results and because it is corrected in the actual simulation result set ((b) and (d)). The following observations can be made about **Fig. 9**:

Voltage: The PFN voltage V_{pfn} in **Fig. 9** (left) practically coincides with the ship's bus voltage V_{dc} (green trace is beneath red trace) while the HESM bi-directional converter controller ramps V_{hesm} about V_{dc} according to (6.4) to produce bidirectional power flows in and out of the HESM.

Current: The ship's current is kept nearly constant during the PFN charge-discharge cycle although it varies non-linearly between a minimum of 2,550 A and a maximum of 2,950 A around an average of about 2,850 A.

Power: The PFN and HESM traces here mirror those obtained in the ideal case. The ship's power, however, is not exactly constant but varies non-linearly between a minimum of 15.5 MW and a maximum of 18 MW around an average of about 17 MW corresponding to the current variation.

Energy: The traces here are very similar to those obtained in the ideal case. The only observation relates to the HESM stored energy (flywheel RPM) which here drifts downward whereas in the case of ideal sources it tended to increase. As was observed previously, this drift is due to minor unbalances neglected in the amp-hour analysis and can be eliminated by proper tracking of N and correction of I_{ship} in (6.4).

6.3 Hybrid Power

This section presents simulation results for the HESM centralized topology using the hybrid power PFN charging shown on the right of **Fig. 4**. Similar to the constant power case, before presenting the simulation results, a value for I_{ship} in (6.4) must is derived according to the following an amp-hour balance.

6.3.1 Amp-Hour Balance

Because the hybrid power variant considers the same centralized HESM topology of **Fig. 2**, the HESM voltage control signal derived in (6.4) remains the same as in the centralized case. The value for the ship current I_{ship} in (6.4), however, must be re-calculated as the waveform of I_{hesm} (**Fig. 6**) in the hybrid charging profile is different than it was for the ramped power charging profile (**Fig. 5**).

The HESM charging-current profile I_{hesm} over one charging cycle of hybrid PFN charging is depicted in **Fig. 6**. This profile shows four time zones denoted T_1, T_2, and T_3. During T_1, I_{hesm} reduces from its peak discharge value of $I_{\min} = I_{ship} - I_{pfn}^{peak}$, reverses direction, and ramps linearly to its maximum charging value of $I_{\max} = I_{ship}$. During T_2, I_{hesm} remains at I_{max} to charge the HESM. During T_3, I_{hesm} decays, reverses, and ramps towards I_{min} to discharge the HESM. During T_4, I_{hesm} remains at I_{min} to supplement I_{ship} during PFN charging.

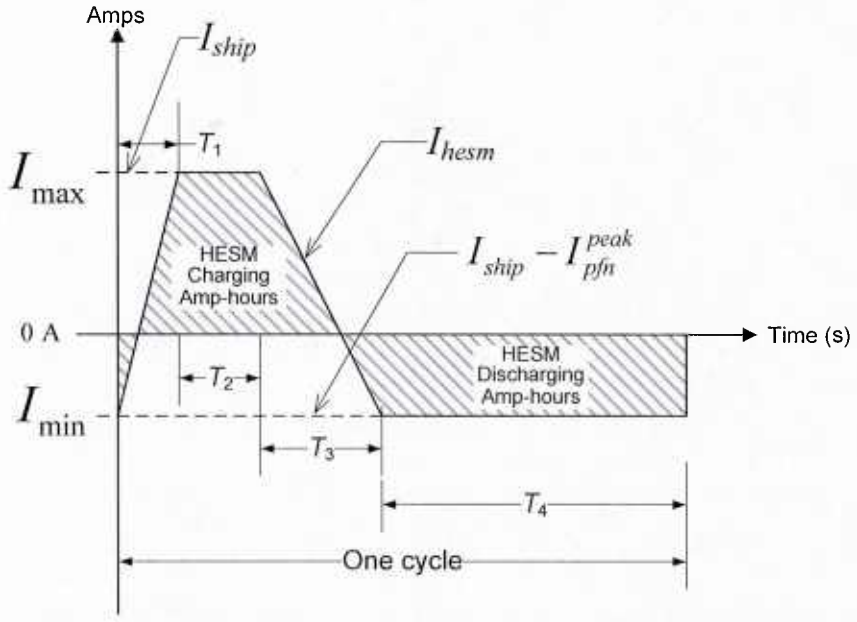

Fig. 6. Amp-hour balance for hybrid power (charging variant 2).

Referring to **Fig. 6**, the value of I_{ship} is estimated by balancing the shaded amp-hour areas as given by (6.11)-(6.12).

$$\int_{T_1}\left(\frac{I_{\max}-I_{\min}}{T_1}t+I_{\min}\right)\mathrm{d}t+\int_{T_2}\left(I_{ship}\right)\mathrm{d}t+\int_{T_3}\left(\frac{I_{\min}-I_{\max}}{T_3}t+I_{ship}\right)\mathrm{d}t+\int_{T_4}\left(I_{\min}\right)\mathrm{d}t=0 \tag{6.11}$$

$$I_{ship}=I_{pfn}^{peak}+\frac{I_{pfn}^{peak}\left(-T_1-2T_2-T_3\right)}{2\left(T_1+T_2+T_3+T_4\right)}\approx 0.725\times I_{pfn}^{peak} \tag{6.12}$$

Substituting T_1=0.25 s, T_2=0.75 s, T_3=1 s, T_4=3 s, and $I_{pfn}^{peak}=22.86\ \mathrm{MW/6\ kV}\approx 3{,}810\ \mathrm{A}$ in (6.12) results in (6.13).

$$I_{ship}\approx 2{,}762\ \mathrm{A} \tag{6.13}$$

I_{ship} in (6.13) is less than it was for the ramped power variant in (6.7). The reduction in I_{ship} reduces the power demand from 17 MW (eq. (6.8)) to 16.5 MW as given in (6.14). In both cases, however, the ship power demand is near the expected 17 MW anticipated by **Fig. 4**

$$P_{ship}=2.762\ \mathrm{kA}\times 6\ \mathrm{kV}\approx 16.5\ \mathrm{MW} \tag{6.14}$$

6.3.2 Simulation Results

Referring to **Fig. 1**, section 6.2.2 presented the result sets for cases (a) and (c). This section presents the result sets for cases (b) and (d).

6.3.2.1 Simulation with Ideal Sources (c)

The simulation results of the hybrid power PFN charging are shown on the *right* of **Fig. 7** and are explained next.

Voltages: Comparing the *left* and *right* side waveforms in **Fig. 7**, there are no noticeable changes in the voltages profiles.

Current: The ship current is similar in both cases: $I_{ship} \approx 2.7$ kA. The *peak* PFN charging current, however, reduced from ~6.6 kA ~3.8 kA. The HESM *charging* current is the same in both charging variants. The peak HESM *discharge* current, however, also significantly reduced from ~3.8 kA to ~1.1 kA. Reductions in current imply less interrupting requirements and cable sizes, but also sustained currents for longer times.
Power: The third curve set shows the same approximate ship power demand as in variant 1: $P_{ship} \approx 17$ MW (really, 16.5 MW in the hybrid power variant). The peak PFN charging power reduced from $P_{pfn} \approx 40$ MW to $P_{pfn} \approx 23$ MW, and the HESM peak power reduced from $P_{hesm} \approx 23$ MW to $P_{hesm} \approx 17$ MW. A contrast of the peak powers in each PFN charging variant is summarized below:

- Ramped power: $P_{ship} \approx 17$ MW, $P_{pfn} \approx 40$ MW, and $P_{hesm} \approx 23$ MW (when discharging)
- Constant power: $P_{ship} \approx 16.5$ MW, $P_{pfn} \approx 23$ MW, and $P_{hesm} \approx 17$ MW (when charging)

Energy: The fourth curve set shows the energy delivered from the ship ring bus as W_{ship} and the energy consumed by the PFN. The energy stored in the HESM is shown in Joules on the left-side vertical axis and in terms of flywheel speed (RPM) on the right-side vertical axis. A noticeable difference in the charging variants is seen in the energy transfer through the HESM. Referring to Fig. 8, the energy transfer in the hybrid charging profile was reduced by ~29 % (100×(27.88-19.68)/27.88=29.41). The hybrid PFN charging (variant 2) reduces the HESM peak power, energy transfer requirement, and the required HESM energy storage.

6.3.2.2 Simulation with Actual Sources (d)

The results of the simulations with actual sources are summarized in **Fig. 9** (right). As can be seen, they reproduce very closely the results obtained with ideal sources in (**Fig. 7**) and the following observations can be made in a manner similar to what was done in the constant current charging case.

Voltage: The PFN voltage V_{pfn} again practically coincides with the ship's bus voltage V_{dc} (green trace is under the red trace) while the HESM bi-directional converter controller varies V_{hesm} about V_{dc} according to (6.4) to produce bidirectional power flows in and out of the HESM. The cycle is different from the ramped power/constant current, but the isolated dc bus voltage remains constant around 6 kV dc.

Current: The ship's current is kept nearly constant (variations less than ±1% of mean) during the PFN charge-discharge cycle although it varies non-linearly between a minimum of 2,570 A and a maximum of 2,870 A around an average of about 2,750 A.

Power: The PFN and HESM traces here mirror those obtained in the ideal source case. The ship's power, however, is not exactly constant but varies non-linearly between a minimum of 15.3 MW and a maximum of 17.3 MW around an average of about 16.4 MW corresponding to the current variation.

Energy: The traces here are very similar to those obtained with ideal sources. The only observation relates to the HESM stored energy (flywheel RPM) which here drifts downward whereas in the case of ideal sources it tended to increase. This drift is again due to minor unbalances neglected in the amp-hour analysis and can be eliminated by proper tracking and correction (when necessary).

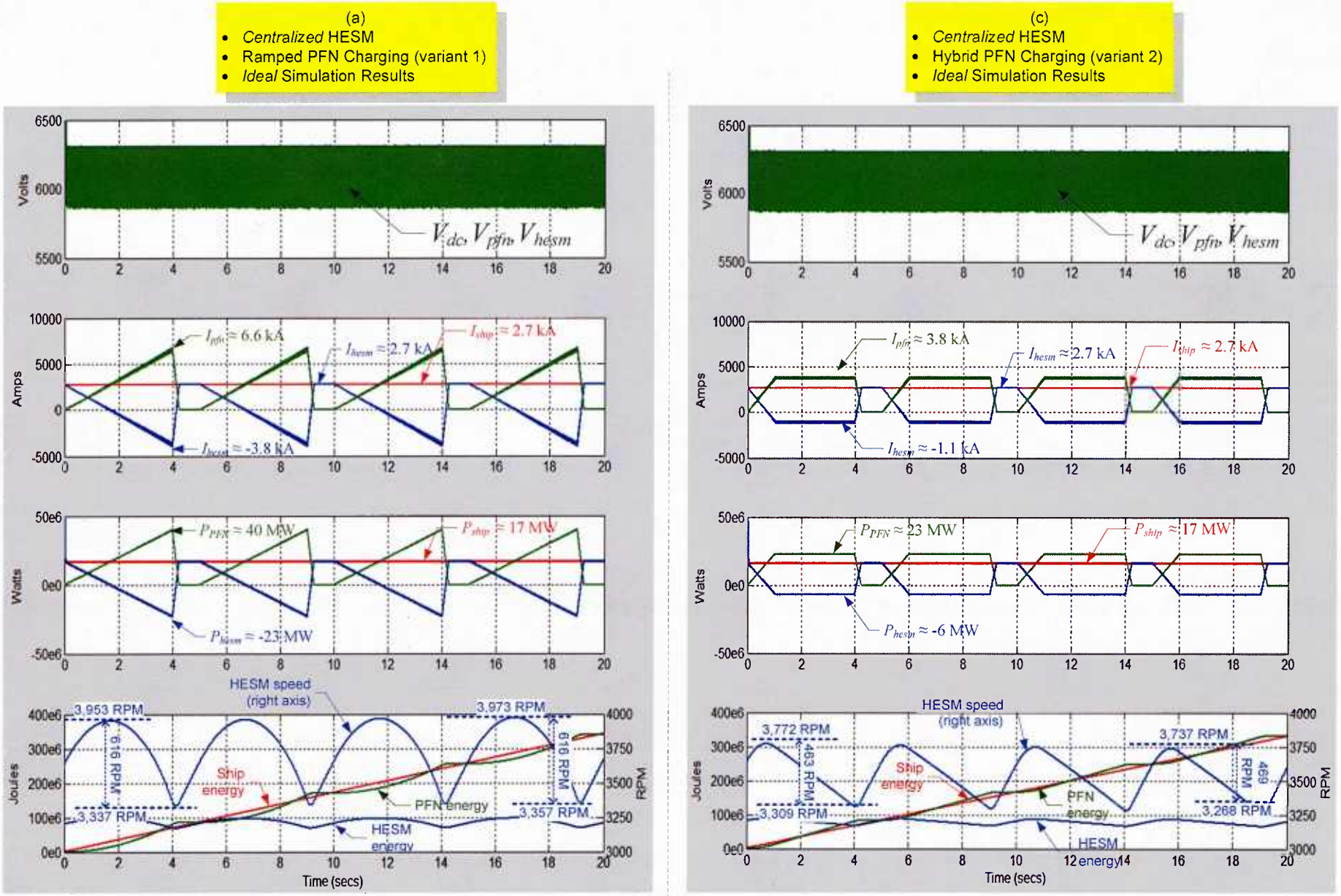

Fig. 7. Ideal simulation results for ramped and hybrid PFN charging variants (centralized HESM). (Actual simulation results are shown in Fig. 9.)

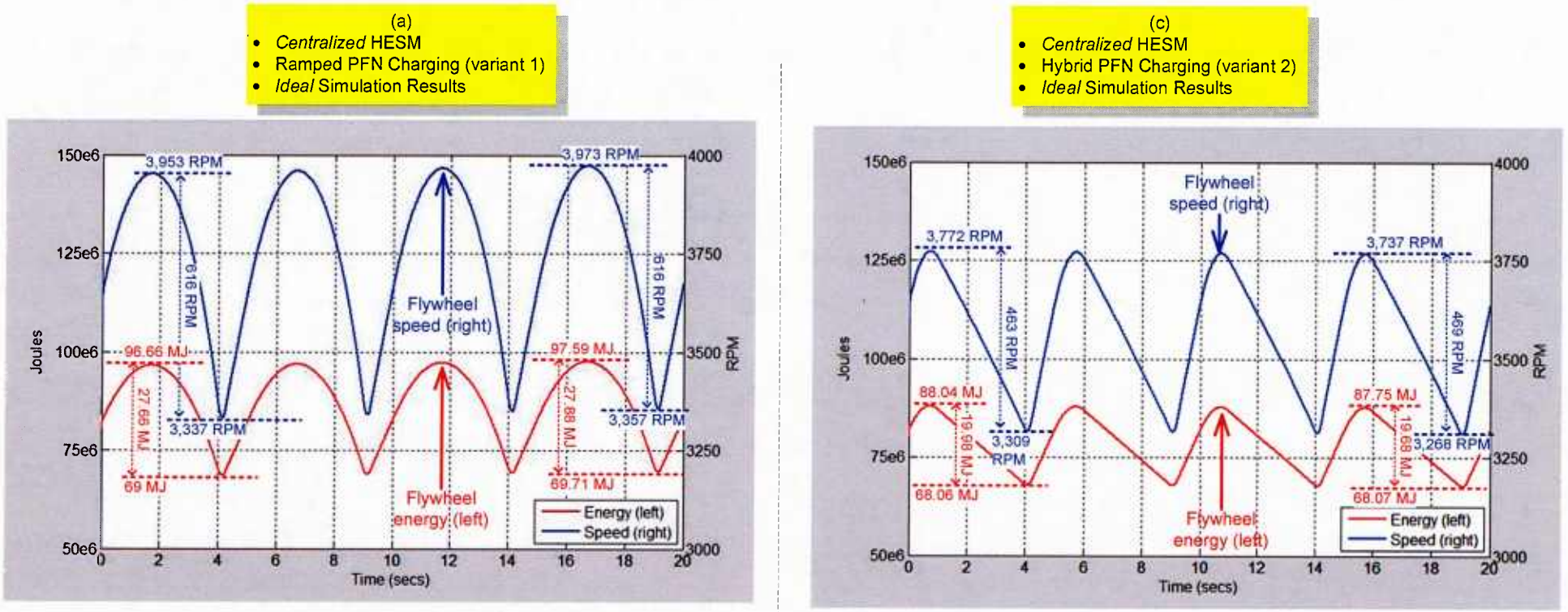

Fig. 8. Ideal flywheel speed and energy for ramped and hybrid PFN charging variants. (Close-up of the lower row of traces in Fig. 7.)

(b)
- *Centralized* HESM
- Ramped PFN Charging (variant 1)
- *Actual* Simulation Results

(d)
- *Centralized* HESM
- Hybrid PFN Charging (variant 2)
- *Actual* Simulation Results

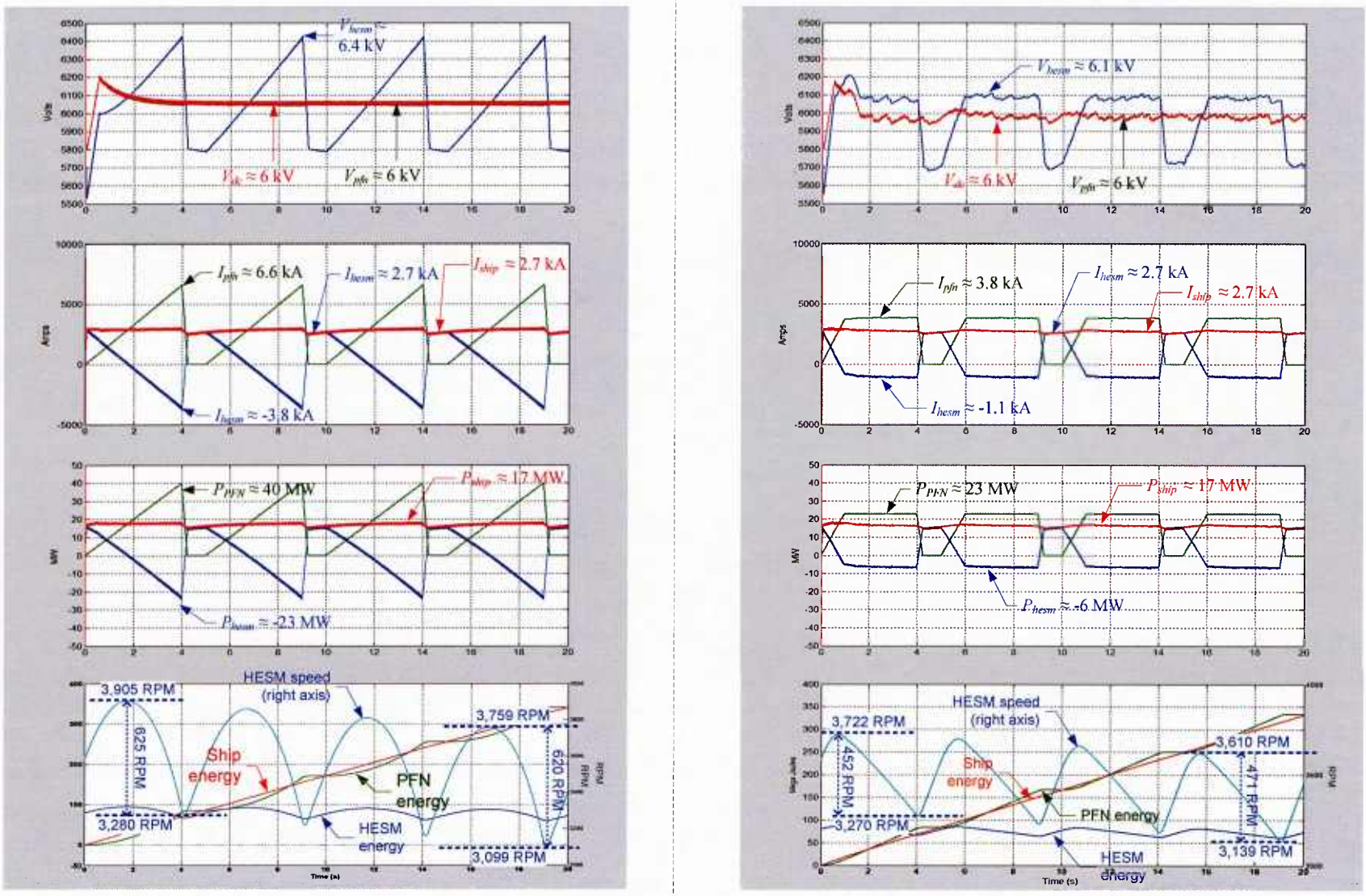

Fig. 9. Actual simulation results for ramped and hybrid PFN charging variants (centralized HESM). (Ideal simulation results were shown in Fig. 7.)

7 Distributed HESMs

This section addresses the right side of the organization diagram presented in **Fig. 1**. Following the procedure illustrated for the centralized HESM unit in Section 6, voltage reference signals are derived first for each HESM bi-directional converter. After these derivations, simulation results are presented to contrast the performance of distributed HESM units over the centralized one. The simulation results include the speed and energy characteristics of the HESM flywheels as well.

7.1 Distributed Voltage Control

Referring to the one-line diagram with distributed HESM units in **Fig. 3**, and for sake of analysis, it is assumed that the voltage around the ring bus is the same. This assumption allows representing the ring bus as a single bus bar and, therefore, to simplify the one-line diagram of **Fig. 3** to the equivalent in **Fig. 10**.

The simplified diagram in **Fig. 10** preserves important characteristics of **Fig. 3**. That is, two generators inject power to the ring bus, one PFN unit connects from the ring bus on its own, and the two HESMs are regarded as distributed instead of centralized. The intermediate bus between the ship ring bus and the HESM units is there to show how the total HESM power and current flow into each HESM unit. The simplified depiction in **Fig. 10** is a common approach [11] to derive control expressions for each HESM bi-directional converter; however, this simplified diagram is not valid for simulation. The simulations presented later in this section are based on the one-line diagram shown earlier in **Fig. 3**.

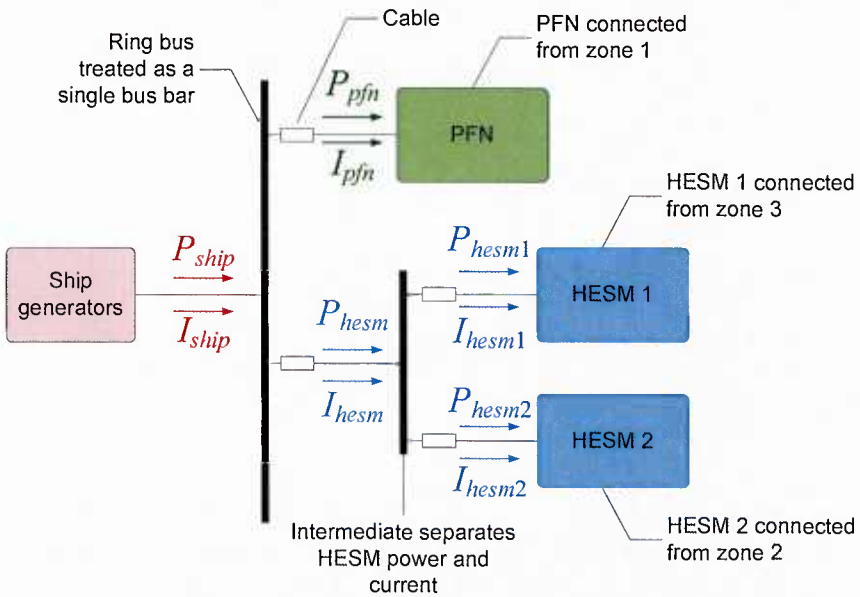

Fig. 10. Simplified representation of ring bus, PFN, and HESM units.

Referring to **Fig. 10**, it is *important* to note that P_{ship} and I_{ship} represent only the contribution of the ship generators toward the PFN and HESM units—that is, P_{ship} and I_{ship} are *not* the total power and current supplied by the ship generators.

The sum of currents at the single-bus bar representation of the ring-bus in **Fig. 10** is given by (7.1).

$$I_{ship} = I_{hesm} + I_{pfn} \tag{7.1}$$

The total HESM current (charging or discharging) is:

$$I_{hesm} = I_{hesm1} + I_{hesm2} = \frac{I_{hesm}}{2} + \frac{I_{hesm}}{2}. \tag{7.2}$$

Substituting (7.2) in (7.1) results in:

$$\begin{cases} I_{ship}/2 = I_{hesm1} + I_{pfn}/2 \\ I_{ship}/2 = I_{hesm2} + I_{pfn}/2. \end{cases} \tag{7.3}$$

Referring to **Fig. 10**, and following the expression stated earlier in (6.2), the current contribution of each HESM can be expressed as (7.4), where V_{dc} is the voltage upstream of each HESM cable, R_{cablei} is the resistance (Ω) of the cable between HESM unit i and its upstream interface bus, and V_{hesmi} is the desired (reference) dc-side output voltage of HESM bi-directional converter i.

$$I_{hesm1} = \frac{(V_{dc} - V_{hesm1})}{R_{cable1}}; \quad I_{hesm2} = \frac{(V_{dc} - V_{hesm2})}{R_{cable2}} \tag{7.4}$$

Substituting (7.4) in (7.3) and solving the voltage reference signal for each HEMS controller results in (7.6) and (7.7) for HEMS units 1 and 2, respectively.

$$I_{ship} = \frac{(V_{dc} - V_{hesm})}{R_{cable}} + I_{pfn} \tag{7.5}$$

$$V_{hesm1} = \underbrace{V_{dc}}_{\text{must be measured}} - R_{cable1}\left(\frac{I_{ship}}{2} - \underbrace{\frac{I_{pfn}}{2}}_{\text{must be measured}}\right) \tag{7.6}$$

$$V_{hesm2} = \underbrace{V_{dc}}_{\text{must be measured}} - R_{cable2}\left(\frac{I_{ship}}{2} - \underbrace{\frac{I_{pfn}}{2}}_{\text{must be measured}}\right) \tag{7.7}$$

Equations (7.6) and (7.7) are the voltage reference signals of HESMs 1 and 2, respectively. These equations also indicate that each HESM will provide (share) one-half of I_{pfn} and that each HESM will charge at one-half of I_{ship}. This $1/M$ current-sharing technique [12] (where M is the number of HESM units) stems from the one-half HESM coefficients introduced in (7.2), which can be adjusted as more HESM units are considered.

Similar to the centralized topology, the voltage controller of each HESM unit must measure the voltage V_{dc} at its upstream bus connection and the total PFN charging current I_{pfn}. The values of I_{ship} required in (7.6) and (7.7) for the ramped and hybrid PFN charging power profiles were derived previously with an amp-hour balance in (6.7) and (6.13), respectively. These values of I_{ship} are the same in the distributed topology as the energy delivered from the ship generators to the HESMs and PFN does not change with HESM topology. Since new values for I_{ship} are not required, the simulation results are presented directly.

7.2 Simulation Results

Referring to **Fig. 1**, section 6.2.2 presented the result sets for cases (a) and (c). Section 6.3.2 presents the result sets for cases (b) and (d). This section presents all simulation results on the right half of the hierarchical chart in **Fig. 1**—that is, to (e), (f), (g), and (h), respectively.

7.2.1 Simulation with Ideal Sources (e)

The ideal simulation results for the distributed HESM topology are shown in **Fig. 11**. These results are compared in two ways:

- Distributed vs. centralized HESM (left of **Fig. 11** vs. left **Fig. 7**, or (e) vs. (a))
- The two PFN charging profiles for the distributed units (left vs. right of **Fig. 11**, or (e) vs. (g))

7.2.1.1 Comparison to Centralized Topology

The following explanations compare the *left* side of **Fig. 7** (centralized HESM) to the *left* side of **Fig. 11** (distributed HESMs).

Voltages: The voltage profile of HESM 1 in **Fig. 11** is closer to the ring bus voltage than was the centralized HESM unit. This is because there is no longer a single feeder serving the entire ship current required by the PFN and HESM units. Instead, the feeder to each HESM unit transmits only ½ of I_{ship}. This lower current reduces the voltage drop in each HESM feeder.

Current: The magnitude of the ship current is unchanged; what changes is its *interpretation.* In **Fig. 7**, I_{ship} represented the ship current flowing in the feeder from zone 1 to the isolated dc bus. (See single feeder to isolated dc bus in **Fig. 2**.) In the distributed case of in **Fig. 11**, Iship represents the combined current *contribution* of both generators, which serves each HESM unit and the PFN. That is, I_{ship} is *not* the total current served by each generator. I_{ship} is the current demanded by the HESM and PFN units together: the current demanded by other loads on the ring bus will continue to be provided by the ship's generators. Here we are focusing only on the fraction of ship's current required by the HESM and PFN. The PFN current, however, is unchanged as in both centralized and distributed cases the PFN remains as a single unit. Both the *charging* and *discharging* currents of each HESM unit are now one half of the values observed for the centralized HESM unit. (In **Fig. 11** all waveforms for HESM 1 and 2 are very similar; thus, the notation HESM 1,2 is used to refer to either HESM unit.) The reduction in HESM current demand favorably impacts cable losses, voltage drop, ampacity requirement, protective device sizing, coordination, and placement. These impacts, however, are not part of this report.

Power: Similar to the current waveforms, the power of the ship and PFN are unchanged. The power of each HESM, however, is one-half the power requirement of the centralized HESM unit. The half-power requirement of each HESM unit, however, requires that both HESM units operate in *unison* to support PFN charging.

Energy: The fourth curve shows that the energy requirement of each HESM unit is approximately one-half of what it was for the centralized HESM unit. This results from assuming one-half of the moment of inertia for each distributed HESM unit. The flywheel's

speed and drifts, however, are similar to what was observed before. A close-up of the flywheel speed and energy is shown in **Fig. 12**.

The following explanations compare result sets (c) and (g), or the *right* side of **Fig. 7** (centralized) to the *right* side in **Fig. 11** (distributed).

Voltages: Similar to the ramped charging profile, the voltage of each HESM unit is much closer to the ring bus voltage than it was before.

Current: The ship current remains unchanged, which means the combined current *contribution* of both generators is the same. This combined ship current, as opposed to the centralized topology, splits into each feeder serving the HESM units and the feeder serving the PFN. The PFN current, however, is unchanged as in both centralized and distributed cases the PFN remains as a single unit. Both the *charging* and *discharging* currents of each HESM unit also reduced to one-half of what was required for the centralized HESM unit.
Power: The power contributed by the generators (P_{ship}) and the power demanded by the PFN (P_{pfn}) do not change. What changes is the charging and discharging power of the HESM unit. The charging and discharging power of each HESM unit are one-half of what they were before.

Energy: The energy requirement for each HESM unit is approximately one-half of what it was for the centralized HEMS unit. This result stems from assuming one-half the moment of inertia for each distributed unit as compared to the centralized HESM unit. The flywheel's speed and drifts, however, do not change. A close-up of the flywheel speed and energy is shown in **Fig. 12**.

7.2.1.2 Comparison of ramped and hybrid charging profiles

The following explanations compare the *left* and *right* sides of **Fig. 11** (result sets (e) and (g)).

Voltages: The voltages are similar in both cases. Due to the high power peaks in P_{pfn} during the ramped charging profile, the voltage at the PFN terminals is slightly reduced. This reduction, however, is contingent on proper conductor selection for the PFN cable (see Table 1).

Current: The ship current I_{ship} and PFN current I_{pfn} are similar in both cases. What changed is the peak charging and discharging HESM currents. Referring to I_{hesm1} (same as I_{hesm2}), the peak discharging current is ~550 A or 28 % of the peak value of 1.9 kA for the ramped charging. The HESM charging current is the same in both charging variants at 1.35 kA.

Power: The third curve set shows approximate power demands for the ship in both ramped and hybrid charging profiles. The peak PFN charging power, in a manner similar to the centralized case (Fig. 7 (a) and (c)), is also reduced from $P_{pfn} \approx 40$ MW to $P_{pfn} \approx 23$ MW with the hybrid charging profile. The hybrid charging profile also reduces the peak HESM power from 11.5 MW to 8.5 MW (per unit).

Energy: The energy stored in the HESM is shown in terms of flywheel speed (RPM) on the right-side axis. Similar to the centralized HESM topology, flywheel speed in the hybrid charging profile reduces the ending swings by ~25 % (100×(631-469)/631=25.67).

7.2.2 Simulation with Actual Sources

The results of the simulations with actual sources are summarized in **Fig. 13** (left) for constant current charging and right for hybrid charging result sets (f) and (h). As can be seen, they reproduce very closely the results obtained with ideal sources (**Fig. 11**) so that the observations made above for the case of ideal sources hold for the case of actual sources as well. Likewise, the comments already made for the case of a single HESM (**Fig. 9**) carry over to the present case of two HESM (**Fig. 11**). The traces for the physical quantities related to each HESM are close and overlap.

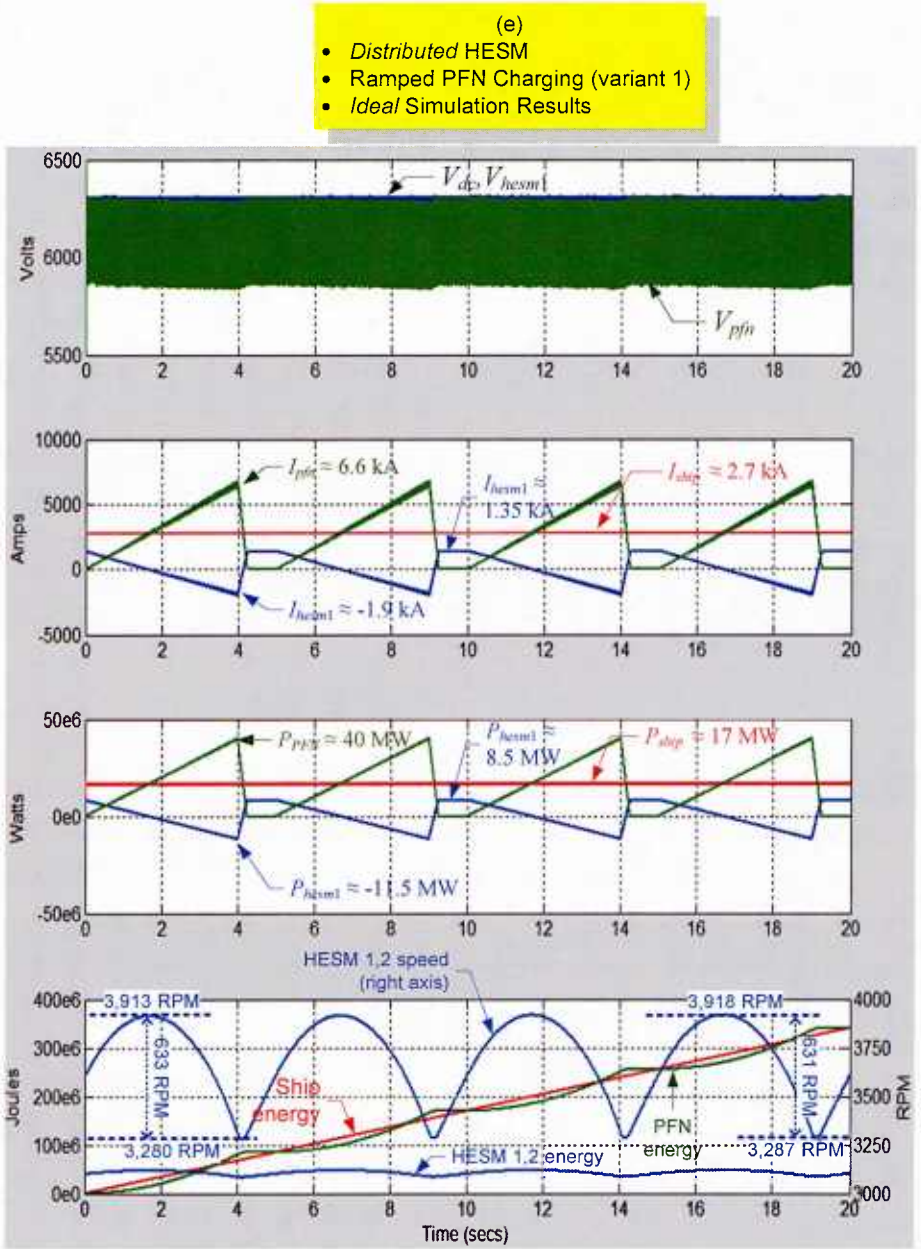

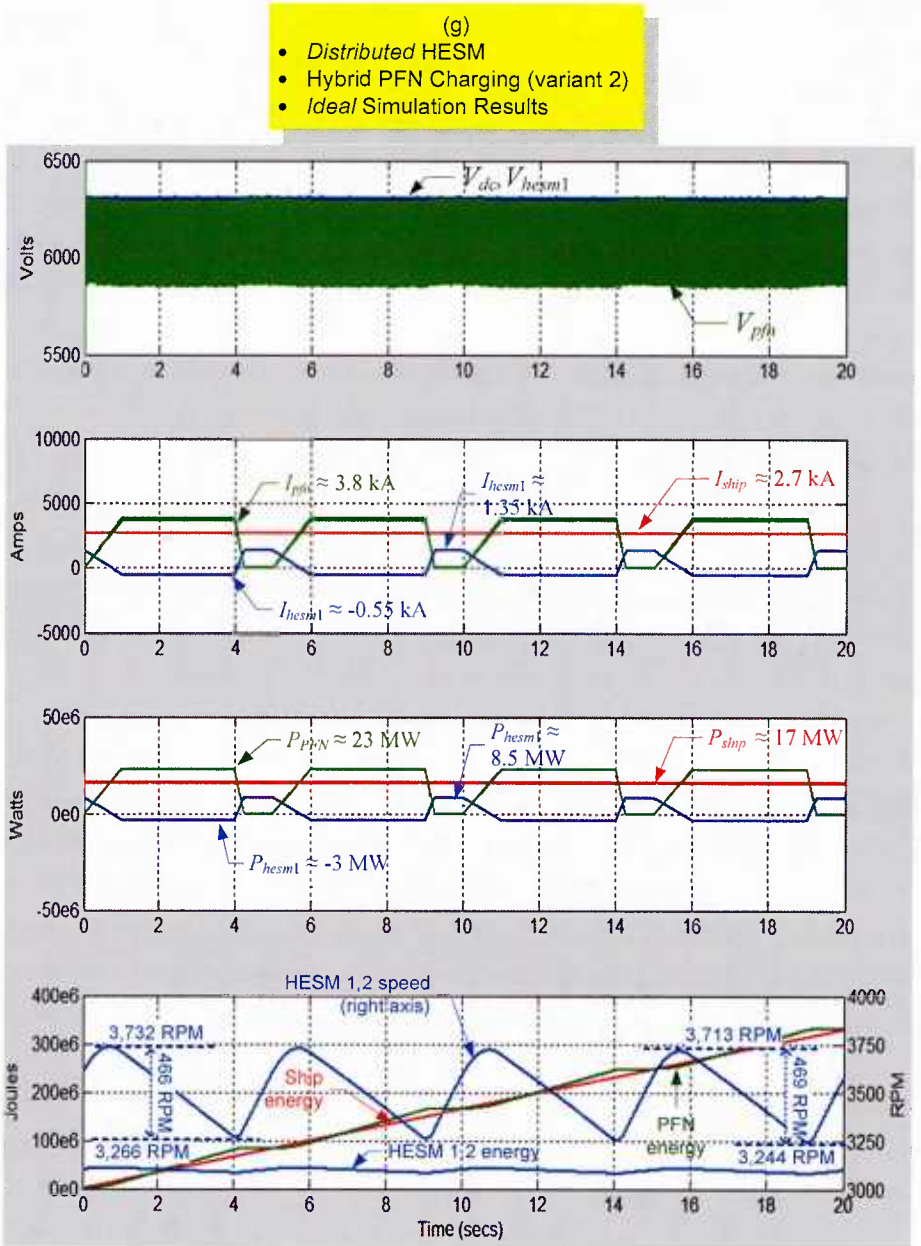

Fig. 11. Ideal simulation results for ramped and hybrid PFN charging variants (distributed HESM). (Actual simulation results are shown in Fig. 13.)

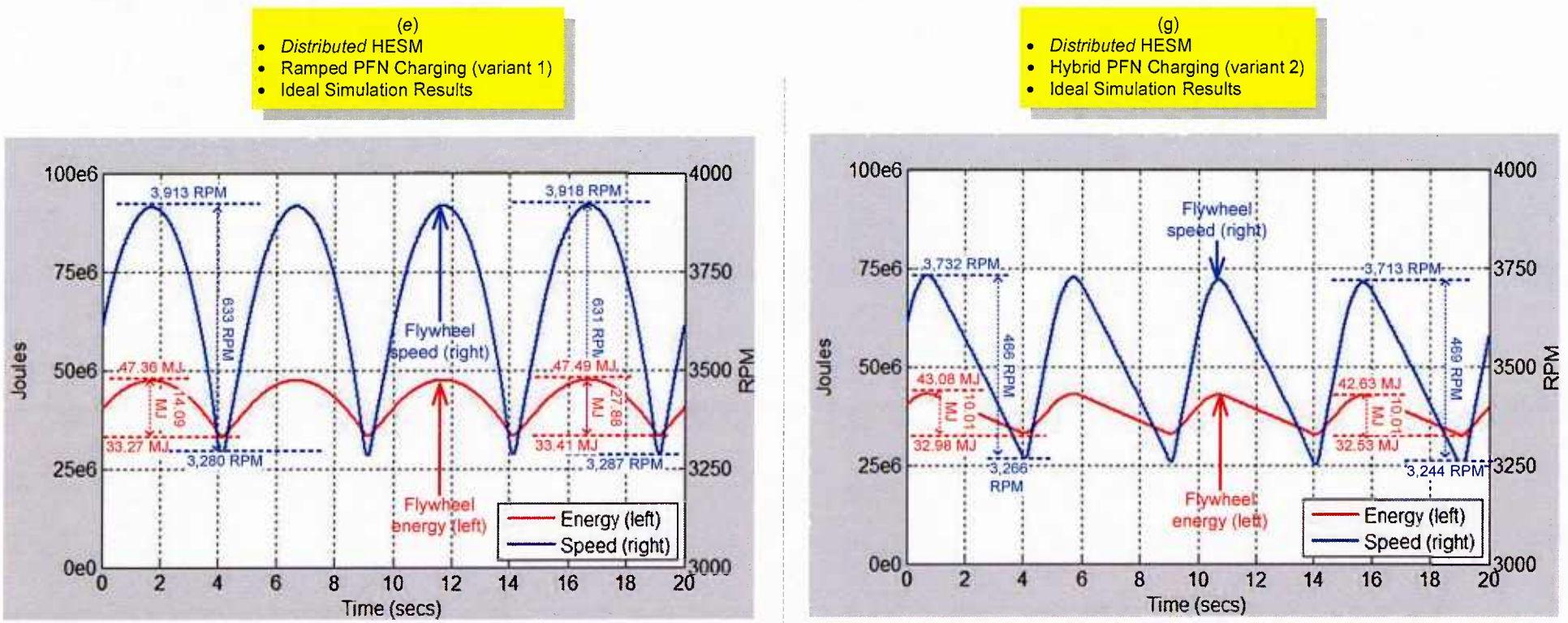

Fig. 12. Ideal flywheel speed and energy for ramped and hybrid PFN charging variants. (Close-up of the lower row of traces in Fig. 11.)

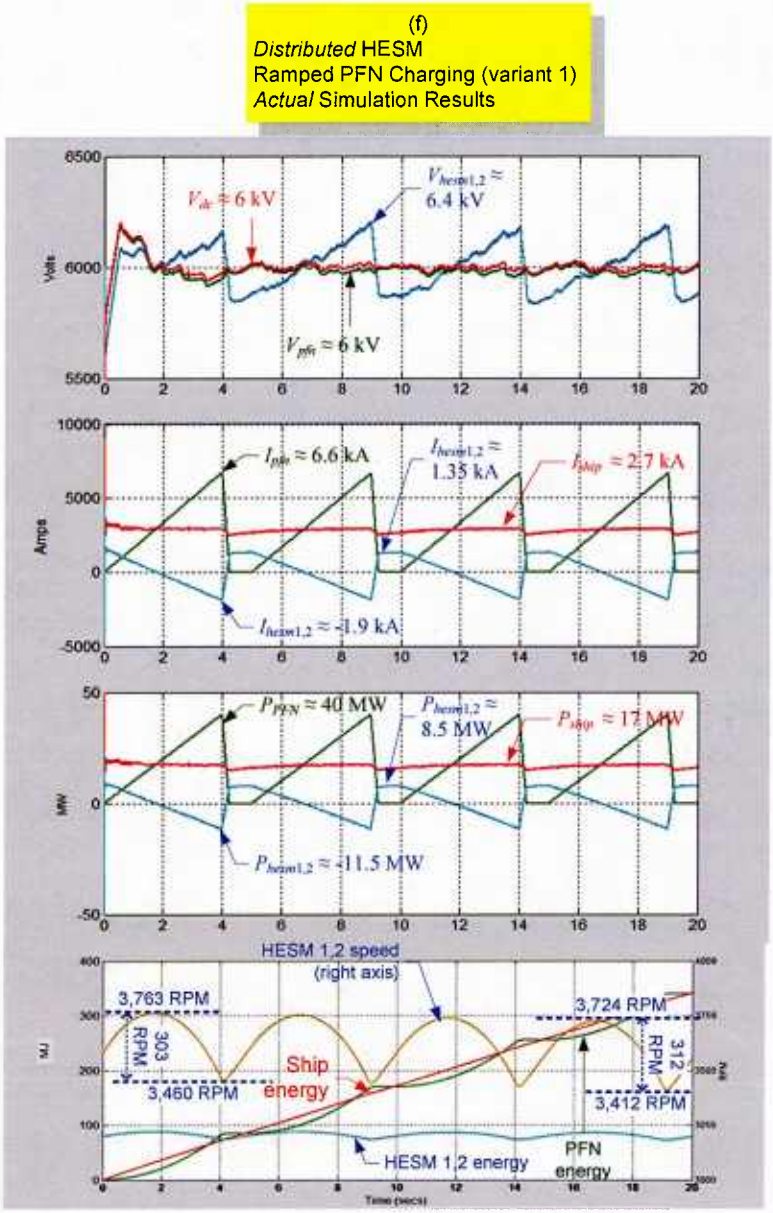

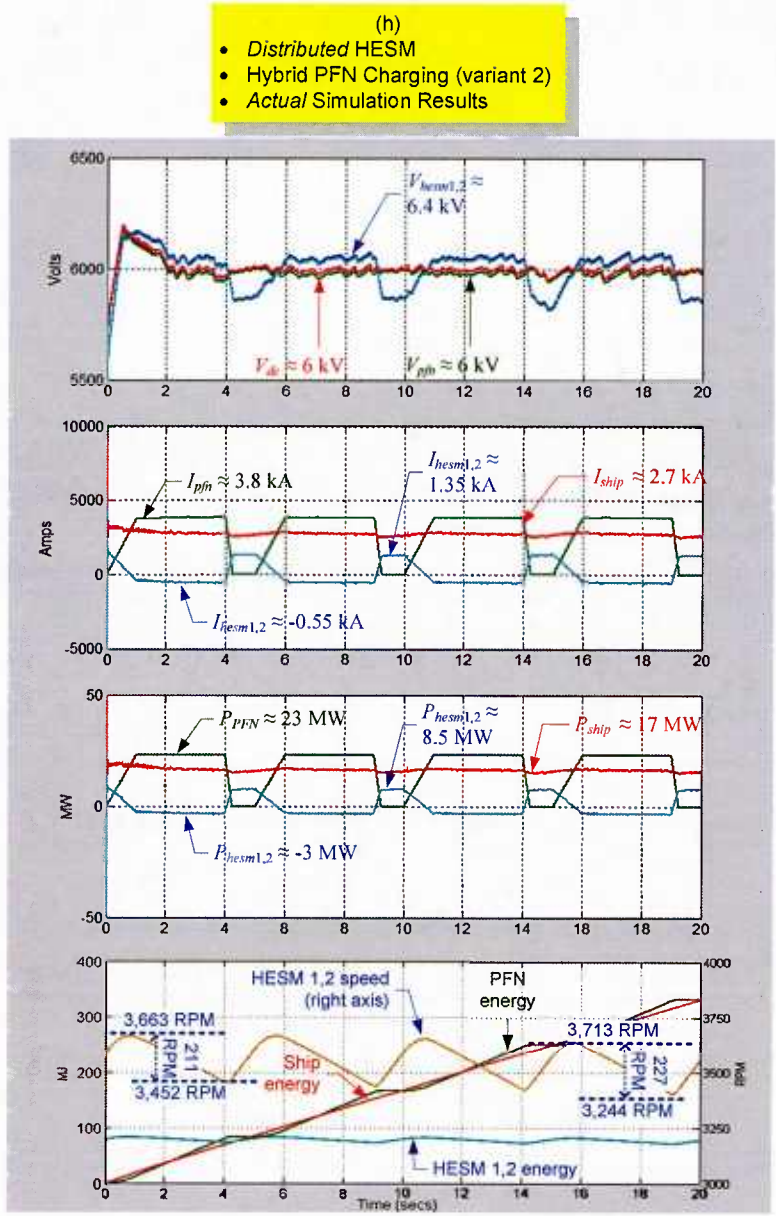

Fig. 13. Actual simulation results for ramped and hybrid PFN charging variants (distributed HESM). (Ideal simulation results were shown in Fig. 11.)

8 Simulation Models

High fidelity simulation models were developed to represent the two architectures and evaluate the performance of the centralized and distributed energy storage modules. Figure 14 shows the top level of one of the models; each major block has operator inputs to characterize the systems under simulation.

The model shown was developed with the assumption of two ship's generators, one PFN with pulsed load, and four HESMs to support the PFN. The modularity of the model allows the user to reposition all elements, generators, PFN, and HESMs, as desired along the ship's power system. For example, the HESMs are shown in Figure 14 distributed around the ship's power bus but could be all located and connected at the same point.

Furthermore, additional elements could be added or some of the existing components could be removed as desired provided some basic control parameters are properly adjusted to account for the changes. This can easily be done by following the instructions in the data initialization input file, also provided with the model. For example and for the convenience of the Navy, a second version of the model shown in Figure 14 was also provided with two generators, one PFN, and two HESMs. Thus, many reference models can easily be generated from the two provided to the Navy. Models with up to eight HESMs have been run successfully, although execution time is strongly dependent on the complexity of the system modeled.

Interesting issues that can be analyzed with the models developed do not only concern the load side of the system but also the source side. Thus, for example, one can study the effect of the transient load at the terminals of the ship's generators and the resulting power quality on the ship's bus to determine, for example, if the limits set forth in MIL STD 1399 are respected..

Likewise, one can monitor how the load is distributed among the generators present when a transient occurs. In this latter case, it was interesting to note that, depending on where the generators, the PFN, and the HESMs were located relative to each other, there was a greater or lesser likelihood that the generators would be sharing the load somewhat equally. In fact, there were cases in which a generator would end up with a disproportionate fraction of the load leading at times even to conditions of overload. Since this is a very real concern, the models were also equipped with an optional power balancing circuit that tries to keep the load equally distributed among the existing generators.

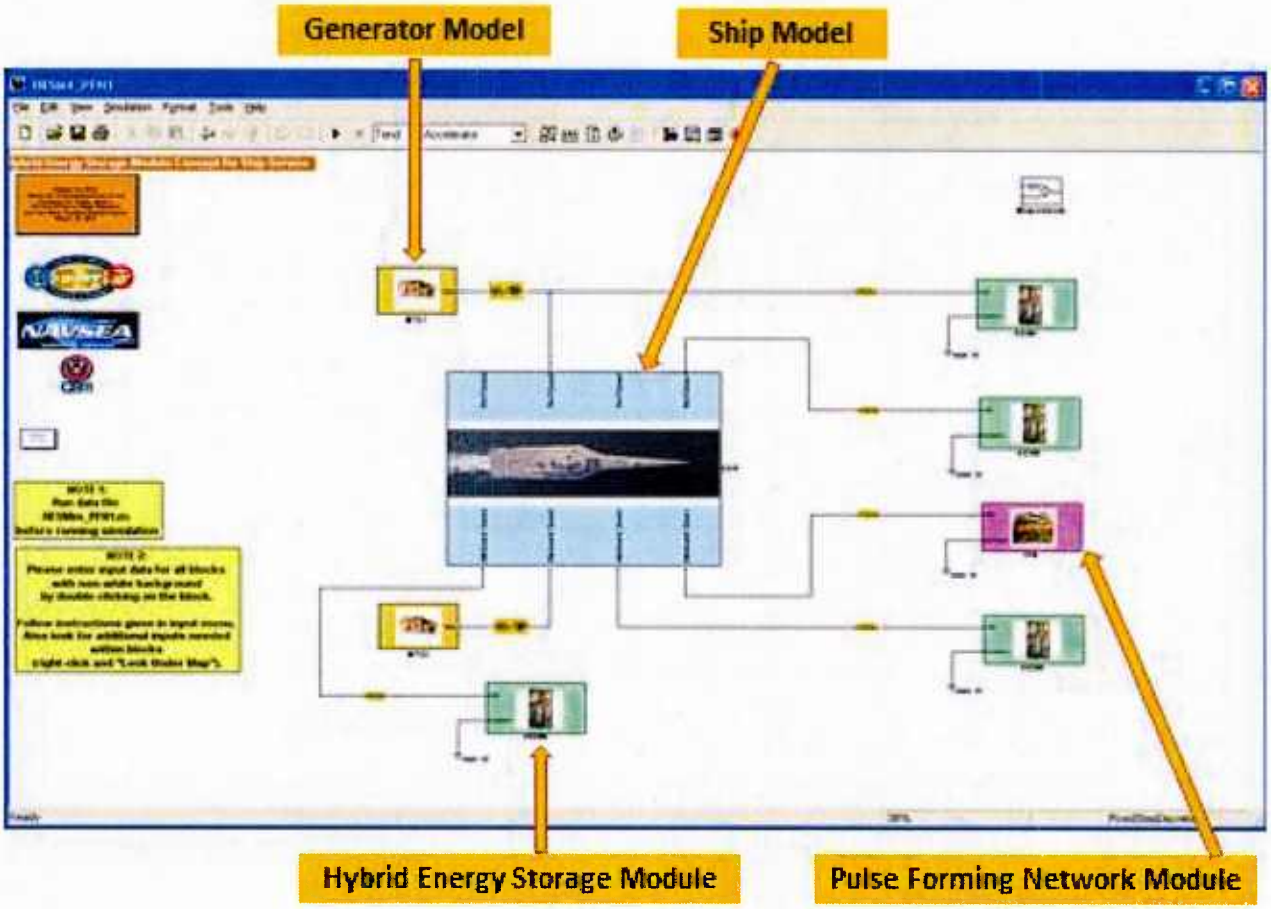

Fig. 14. One of the two reference MatLab Simulink models for the study of the effect of HESMs and a pulsed load on a ship's power system.

Annotated simulation models are attached to this report as Appendix 1.

9 Machine Characteristics

The power and energy delivery parameters identified through the simulations run sets ((a) through (h) in **Fig. 1**) provide initial insights into the design of the HESM flywheel battery: the combination of the rotating inertia and the electric machine required to charge and discharge the energy store. The final design of the rotating machine for the HESM will require additional analysis. Based on the initial simulation results in **Fig. 7**-**Fig. 9** (result sets (a) through (d)), the peak power rating for the HESM ranges from approximately 23 MW for the constant current/ramped power charging profile to about 17 MW for the hybrid charging profile. The energy transfer energy from the HESM ranges from approximately 28 MJ (left side in **Fig. 8**) for the constant current/ramped power charging profile to about 20 MJ for the hybrid charging profile (right side of **Fig. 8**).

Using the ratio of peak power to delivered energy as a figure of comparison, the constant current/ramped power profile has a power to energy ratio of 1.42 and the hybrid charging profile has a power to energy ratio of 0.85. In contrast, a flywheel battery for a typical vehicular or UPS application will have power to energy ratios at least an order of magnitude lower; for example, two hybrid-electric vehicle flywheel programs at UT have power to energy ratios of 0.02 and 0.004. These figures indicate that the HESM design is heavily driven by the power requirement of the system as opposed to the amount of stored and delivered energy. Electrochemical batteries are not well suited for this type of power and energy profile -- they are generally more appropriate in applications with a lower power to energy ratio. (This characteristic may change if the HESM is used to provide energy storage for other shipboard applications such as UPS for single generator set operations.)

The HESM power requirements primarily impact the design of the motor/generator and the power converter; however, the optimum HESM design must consider a system-level optimization of all three major elements of the HESM system including the rotating inertia, the motor/generator, and the bi-directional power converter. The following sections present the critical design issues for each element.

9.1 Power Conversion Equipment

The motor/generator maximum operating speed will be limited by the characteristics of the bi-directional power converter – the converter must be able to provide the required power at the fundamental frequency to match the speed and pole count of the motor/generator. Although it increases the fundamental frequency required for a given speed, a higher pole count is desirable because, for a given power rating, the power density of the machine will tend to increase as the number of poles increases [13].

In general, the frequency capability of a power converter will decrease as the power rating of the converter increases. However, the design can take advantage of increased phase counts for the driven rotating machine, and a higher power motor can be driven using multiple smaller converters. For example, a 12-phase, 16 MW motor can be driven by an array of four three-phase converters, each with a nominal rating of 4 MW. This approach also potentially offers increased reliability – if one converter module fails, the motor can continue operation at reduced power. Moreover, this approach also applies to architectures based on dc or ac distribution

systems since the intermediate dc link of ac-ac converters provides the compensating point for the phase shifts among the parallel three-phase units.

Although silicon-carbide and gallium-nitride semiconductor technologies offers the promise of significant increases in converter performance, these technologies are not yet mature enough for critical DOD applications. For the purposes of this study, it is assumed that the design will be limited to a maximum fundamental operating frequency of 500 Hz and that multiple converter modules will be used to drive higher power machines. Given the anticipated adoption of wide band gap semiconductor switching at higher speeds, this should be considered a lower bound on the future capability.

9.2 Machine Considerations

The inertia of the HESM flywheel rotor will define the maximum stored energy at a given angular velocity:

$$W = \frac{1}{2} J \omega^2 \tag{8.1}$$

where

W = energy stored in flywheel mass [Joules]
J = moment of inertia [kg-m^2]
ω = flywheel speed [rad/s].

Assuming a depth of discharge of 50% of maximum speed, the energy transferred from the flywheel storage is equal to 75% of the maximum stored energy. This also means that, knowing the minimum amount of energy that must be transferred, we must design the machine such that *the stored energy is at least 33% larger than the delivered energy.* This figure defines the minimum energy storage at maximum operating speed; the actual energy storage will likely be larger than this value. Depths of discharge below this value offer diminishing returns and increase the challenges for the motor/generator to make required voltage at the lower speeds.

While energy storage flywheels allow independent selection of energy and power, the design of the HESM inertia cannot be defined without consideration for the characteristics of the motor/generator and power converter. The squared relationship of energy with angular velocity drives the design towards the highest practical rotational speed to maximize energy density; however, the relatively high peak power of 17 to 40 MW effectively limits the minimum physical size and maximum operating speed of the motor/generator. (The peak power values are of relatively short duration so the designs can be more aggressive than machines rated for continuous duty at these power levels.) This can be illustrated by consideration of the maximum practical tip speed of the flywheel and motor/generator and the effective torque generated per unit surface area or unit volume of the motor/generator.

Tip speed simply refers to the product of angular velocity and outer radius of the rotor. UT has demonstrated high performance graphite epoxy composite flywheels at tips speeds in excess of 1,350 m/s and small devices have reached tip speeds of over 2,000 m/s.[4] In contrast, the

[4] http://www.rct-systems.com/Power-Systems-Division/Machinery-0024amp;-Magnetics.aspx

weight of permanent magnets or windings limits the maximum practical tip speed for an electric machine to approximately 3-400 m/s. For flywheel applications, the speed decreases as you extract energy from the rotor so motor/generator must be capable of the required performance at the minimum speed of the machine. These constraints, in conjunction with electromagnetic and rotor dynamic considerations, define the size of the motor/generator.

Torque generation in an electric machine is described by the following relationship:

$$T \propto B \times A_s \times L \times D^2 \tag{8.2}$$

where

T = torque [N-m]
B = air gap flux density [Wb/m^2]
A_s = stator line current density [A/m]
L = active length [m]
D = air gap diameter [m].

The air gap flux density is set by the B-H (magnetic flux density vs. intensity) characteristics of the iron in the rotor and stator and by the available magneto-motive force (MMF) of the excitation source (the strength of permanent magnets or the allowable current or current density in the field windings). In slotted structures, the flux density in the teeth is approximately twice that of the air gap so for a typical saturation limit of 1.8 T, the peak field in the air gap is limited to approximately 0.9 T_{peak}, or about 0.57 T rms.

The diameter of the air gap is maximized to take advantage of the squared relationship but is limited by the practical consideration of the 3-400 m/s tip speed limit. The length of the rotor is effectively constrained by rotor dynamic considerations—as the rotor gets smaller in diameter and longer, its stiffness is not adequate to allow sub-critical operation at high speed. This is particularly important for flywheel applications where the speed is changing during every charge/discharge cycle. Supercritical rotors may require negotiation of the critical speeds on every cycle.

The torque being generated at the rotor surface can be linked to the volume of the rotor [14]:

$$TRV = \frac{T}{\pi r^2 l} \tag{8.3}$$

where

TRV = torque per unit rotor volume (kN-m/m^3)
T = torque generated (kN-m)
r = rotor radius (m)
l = active length (m).

If one considers the tangential force generated by the $J \times B$ interaction of the current and magnetic field in the air gap and the surface area of the rotor, an effective electromagnetic "shear stress" can be calculated. Referring to the "shear stress" as sigma, σ, this parameter can be related to the torque generated per unit rotor volume, TRV as:

$$TRV = 2\sigma \tag{8.4}$$

where

σ = shear stress in kN/m^2.

High performance, liquid cooled electric machines typically demonstrate shear stresses on the order of 70 -100 kPa and TRV values between 130 and 220 kN-m/m^3.

Using these relationships, one can begin to estimate the size of the motor generator as a function of minimum rotor speed. Thus, from rotor angular velocity and for a given tip speed the rotor radius can be calculated.

Furthermore, recalling that:

$$P = T \cdot \omega \text{ or } T = \frac{P}{\omega} \tag{8.5}$$

where

P = power [W]
T = torque [N-m]
ω = angular velocity [rad/s],

Fig. 15 shows the calculated torque for a variety of operating speeds for a single HESM as well as for multiple units.

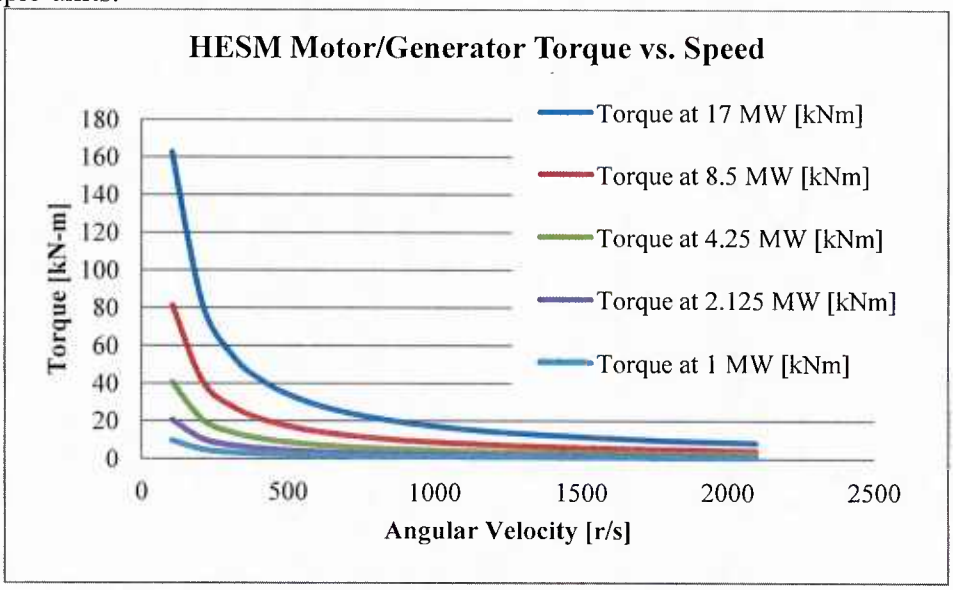

Fig. 15. Torque–speed curves for motor/generator sets of different size.

Using these torque values and a representative value for effective shear stress, one can calculate the required surface area of the motor/generator rotor and from this, since the radius is already known, the rotor length can be derived. Then the rotor moment of inertia and the energy stored in the rotor can be calculated.

Proceeding in this fashion, one can make the following preliminary estimates:

1. A single HESM unit with a rotor radius of 40.9 cm, a rotor length of 25.6 cm, spinning at 7,000 RPM (467 Hz from the converter for an 8-pole machine) can store a maximum of 23.8 MJ and operates at 17 MW.

2. Two HESM units with a rotor radius of 40.9 cm, a rotor length of 12.8 cm, spinning at 7,000 RPM (467 Hz from the converter for an 8-pole machine) can store a maximum of 11.9 MJ and operate at 8.5 MW. Thus the combined performance of the two units is equal to that of the single HESM.

Another possibility is:

1. A single HESM unit with a rotor radius of 23.9 cm, a rotor length of 43.9 cm, spinning at 12,000 RPM (400 Hz from the converter for a 4-pole machine) can store a maximum of 13.9 MJ and operates at 17 MW.
2. Two HESM units with a rotor radius of 23.9 cm, a rotor length of 22.0 cm, spinning at 12,000 RPM (400 Hz from the converter for a 4-pole machine) can store a maximum of 7.0 MJ and operate at 8.5 MW. Once again, the combined performance of the two units is equal to that of the single HESM.

Likewise, more combinations can be considered. It can be noticed that the performance of the first system so estimated comes very close to fulfilling all requirements for our HESM system operated in the hybrid charging mode. Thus, essentially no external flywheel is necessary in addition to the energy stored by the HESM rotor itself, provided the rotor is made a little longer than required to deliver the required power. This is quite feasible, since the aspect ratio (length/diameter) of the rotors calculated above is substantially less than 1.0 (0.313 and 0.157 respectively).

Conversely, the second system estimated above, will need additional inertia to fulfill the requirements of our HESM. In this case, however, the aspect ratio of the machine's rotors calculated above is closer to 1.0 (0.92 and 0.46 respectively) and, thus, will likely lead to a better design from the standpoint of volumetric power density.

9.3 Machine Sizing Study

The goal of this task is to quantify the trade-offs for the number of flywheels relative to the total size and mass devoted to flywheel energy storage using detailed sizing studies based on previous UT-CEM flywheel programs.

The following Figure 16 summarizes the various flywheel designs developed at UT-CEM and highlights the two models used for this initial sizing study.

Data is For Official Government Use Only														
Mechina Name	Peak Power (kW)	Continuous Power (kW)	Rotor Energy (MJ)	Rotor RPM	Rotor Design	Tip Speed at Full Energy (m/s)	Depth of Discharge (energy, %)	Mass of Power Electronics	Mass of Flywheel Module (incl motor-gen) (kg)	Power Electronics Dimensions (m)	Flywheel Module Diametar (m)	Flywheel Module Length (m)	Project Status	Comments
EMAL6	60,000	n/a	117.0	4,200	Partially integrated, cylindrical, mass loaded, non-composite	240	75%		19,273		1.75	3.10	Built	EMALS is a synchronous machine (the energy store) with an 800 kW exciter and a 1.2 MW induction motor to re-accelerate the machine after the discharge, all in line on the same shaft. Is a pulse power machine. The electronics were not part of CEM's effort.
ALPS	4,000	2,000	478.8	15,000	Non-integrated, cylindrical, composite	990	75%	3,000	13,400	2 x 2.3 x 1.4	1.64	1.86	Built	ALPS is a non-integrated machine, with the motor generator separate form the energy storage rotor.
Transit Bus	250	110	7.2	40,000	Partially integrated, cylindrical, composite	935	75%		250	0.7 x 0.5 x 0.2	0.70	0.75	Built	Machine was capable of 250 kW, but power electronics were only capable of 150 kW. Machine weight does not include containment or gimbals.
CHPS	10,000	350	25.2	20,000	Fully integrated inside out, mass loaded, composite	800	75%	112	480				Designed through CDR	Duel purpose machine, with 5MW rating for pulse weapons and 350 kW for hybrid electric combat vehicle load leveling.
FESS	5.0	3.8	13.0	53,000	Partially integrated, cylindrical, composite	920	88%		115				Designed thru CDR	Design focus on high efficiency (>94% turn around efficiency for flywheel)
Small Cal	864,000	n/a	9.0	25,000	Composite, cylindrical, mass loaded	502			850		0.40	0.43	Built	Pulse power machine
Cannon Cal	2,400,000	n/a	39.6	12,000	Composite, cylindrical, mass loaded	458	50%		865		0.73	1.00	Built	Pulse power machine
Sub Scale	3,000,000	n/a	23.0	12,000	Composite arbor, composite rotor	380			2,400		0.80	1.00	Built	Pulse power machine
AIR	73,000	n/a	6.2	6,400	All Iron Rotor								Built	Pulse power machine
Iron Core	1,000,000	n/a	37.8	4,700	Iron	200			10,000		0.80	1.00	Built	Pulse power machine
HVHP	125,000	n/a	3.25	8,600	Aluminum	220					0.84		Built	Pulse power machine; homopolar machine
BHPG	90,000	n/a	10.0	6,073	Iron	181			8,000		0.57	0.59	Built	Pulse power machine; homopolar machine

Fig. 16 UT-CEM flywheels and the two models selected for the initial sizing study. The BUS flywheel is a partially integrated design and the CHPS machine is a fully integrated design.

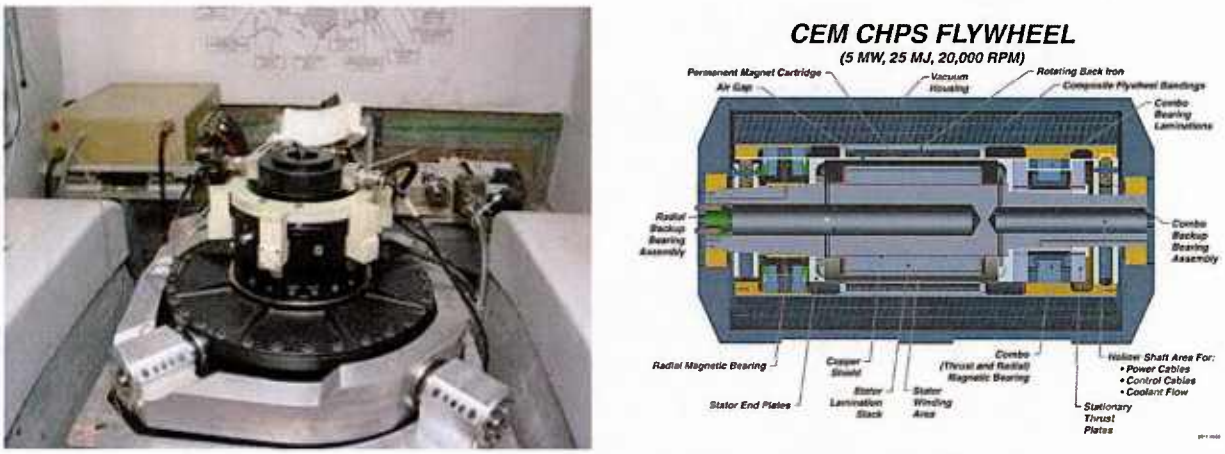

Fig. 17 BUS and CHPS flywheel batteries used in initial sizing study.

Matlab Simulink models were developed as a design tool to calculate the size and weight of flywheel rotors over a range of energy and power ratings for the two topologies presented above. The rotor sizing tool was validated against the actual rotor designs for the two programs. Figures 18 and 19 show representative models of the two flywheels used for the validations.

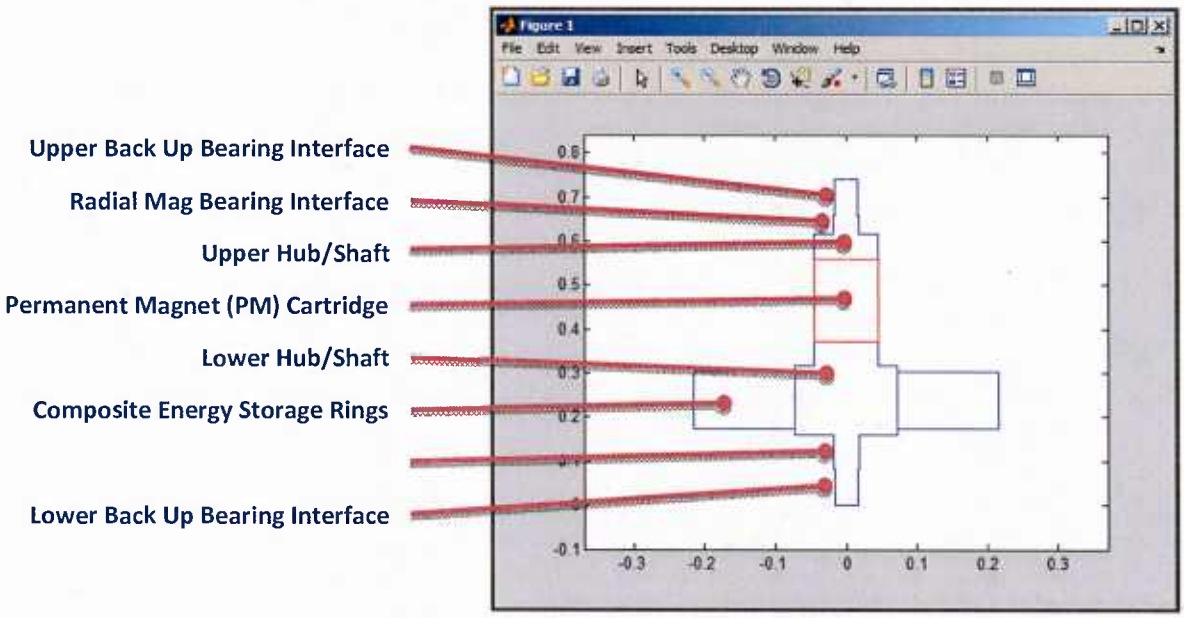

Fig. 18 Rotor sizing tool for partially integrated flywheel design.

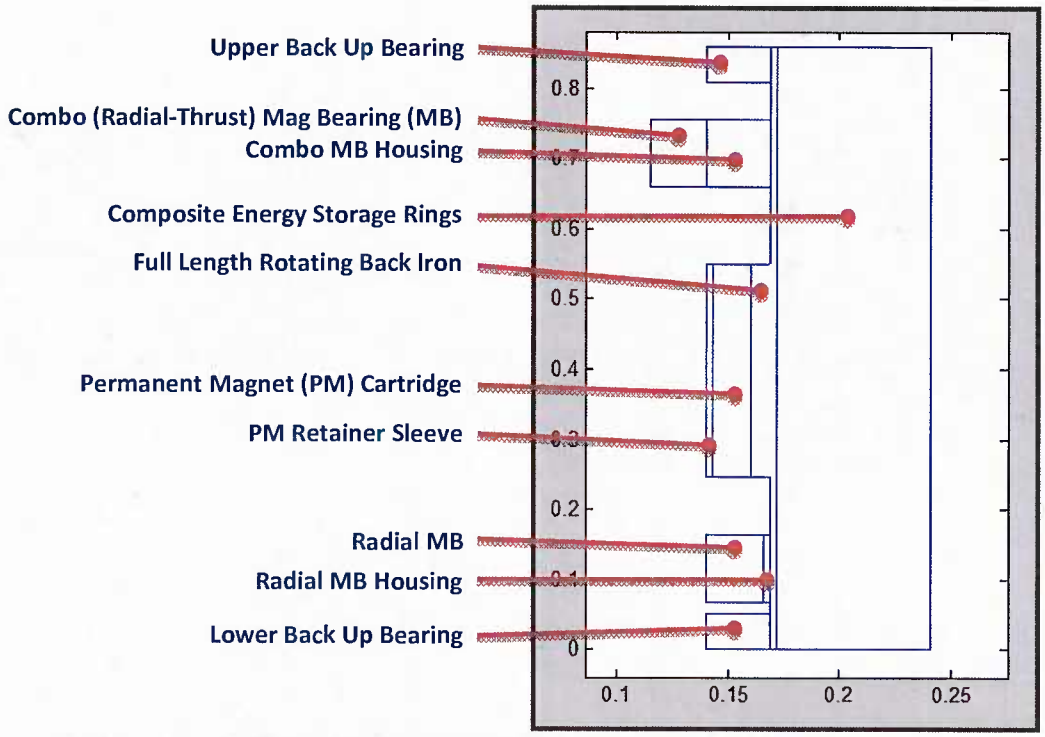

Fig. 19 Rotor design tool for fully integrated flywheel design.

Based on the results of the initial evaluations using the rotor design tool, a more detailed study was conducted using the CHPS baseline design topology. There are two strong indications that the CHPS flywheel design can provide an approach to meeting the baseline HESM requirements with only two machines that each can fit through a 26 inch (0.66 m) hatch.

- Use TRV scaling approach to show that CHPS topology and envelop is within the state-of-the-art (referred to as "*TRV scaling*" approach).
- Use CHPS program plots to provide a direct path to meet HESM requirements by adding an extra energy storage ring, which increases flywheel housing OD from 22 inches to 24 inches (referred to as "*added composite ring*" approach.

For comparison with the HESM requirements based on hybrid charging profile:

- HESM required power (occurs during flywheel charging): 17 MW (8.5MW per machine)
- HESM rms power required: 9.3 (4.65 MW_rms per machine)
- HESM required delivered energy: 20MJ (10MJ per machine)

Baseline CHPS design is good match with ~25% depth of discharge:

- w_{max} = 20,000 RPM; w_{min} = 14,859 RPM
- Power at w_{min} = 8.52MW
- E_{wmax} = 24.59 MJ; E_{wmin} = 13.57 MJ; Energy Delivered = 11 MJ

The CHPS machine was originally designed for operation with a resonant converter that allowed for higher performance than is projected by the TRV evaluation. The system is very attractive for mobile or space constrained applications due to the high volumetric energy and

power density of the custom power supply. Figure 20 shows the components of the CHPS power supply to scale; the OD of the CHPS flywheel battery will fit through a 26" hatchway.

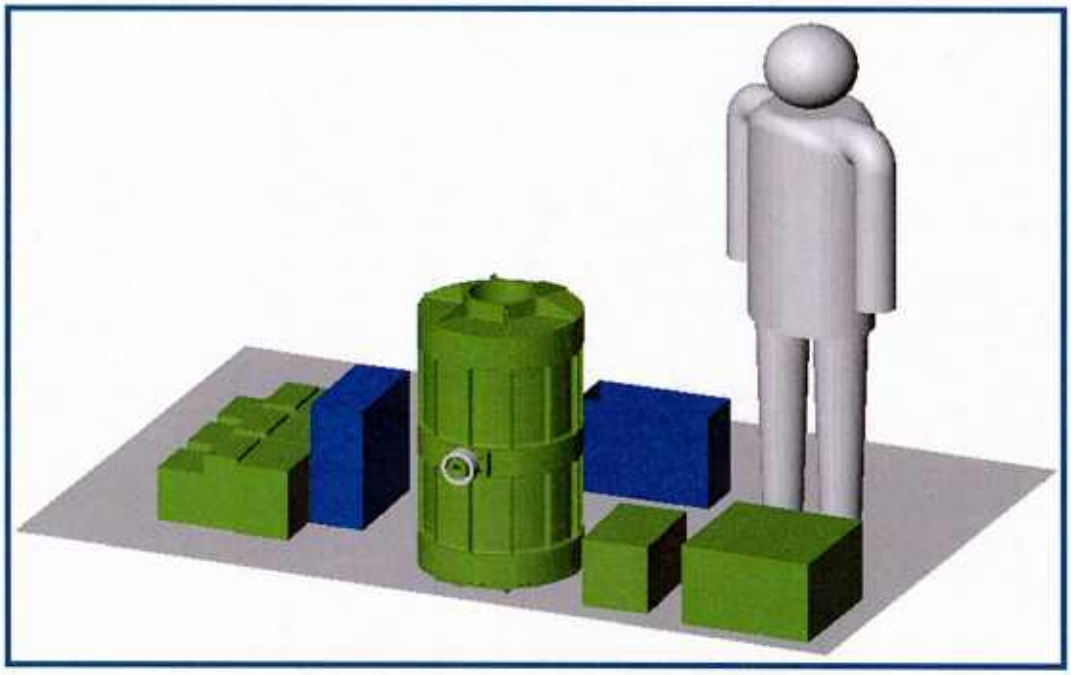

Fig. 20 CHPS power supply components to scale.

Output power is not linear with rotor speed due to resonant output circuit so, for the second design evaluation, the HESM was projected using data from the power/speed curves including a custom resonant converter. Figure 21 shows the power and efficiency performance as a function of stored energy (rpm), into a resistive load including saturation effects.

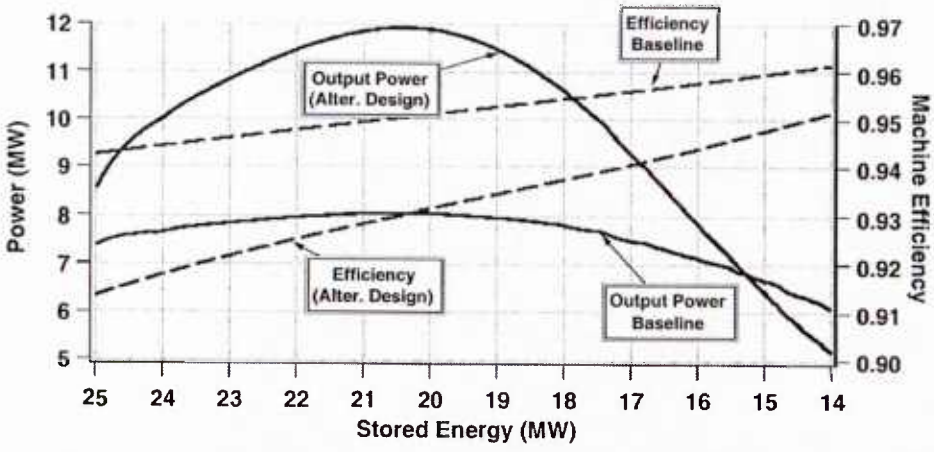

Fig. 21 Power and efficiency as a function of stored energy into a resistive load including saturation effects.

For this design, an additional flywheel ring was also incorporated onto the rotor to increase the inertia and stored energy. Due to the high tip speed of this application, the composite ring is constructed of high modulus T1000G graphite/epoxy composite. The strains in the outer composite ring are well within demonstrated performance and have significant margin at the

operating point required for the HESM application. This implies that additional gains in stored energy are possible, albeit at the expense of reduced structural margin and increased risk. Table 2 summarizes the strain and stress characteristics of the added T1000G flywheel ring.

Table 2. Stress and strain of T1000G flywheel ring over operating temperature range.

	75°F			0°F			225°F			Factor of Safety
	0 rpm	15 krpm	20 krpm	0 rpm	15 krpm	20 krpm	0 rpm	15 krpm	20 krpm	
F1 radial compression	-13.3	-14.6	-17.7	-11.1	-12.4	-16.7	-17.9	-19.2	-20.3	2.2
axial tension	3.4	3.4	3.3	3.6	3.5	3.4	2.2	2.1	2	3.9
rz shear	2.6	2.8	3	2.1	2.3	2.5	3.9	4.1	4.3	1.9
hoop strain	0.0019	0.0037	0.0061	0.0018	0.0037	0.0061	0.0024	0.0041	0.0061	2.3
F2 radial compression	-5.7	-5.5	-6.6	-4.7	-4.6	-5.8	-7.7	-7.5	-7.8	5.8
axial tension	2.7	2.2	2.7	2.8	2.9	3.4	2.4	2	1.7	4.1
rz shear	1.8	2	2.1	1.4	1.6	1.9	2.5	2.7	2.8	2.9
hoop strain	0.0021	0.0035	0.0052	0.0019	0.0033	0.005	0.0027	0.0041	0.0056	2.5
F3 radial compression	-0.81	-0.72	-0.78	-0.71	-0.62	-0.68	-1.1	-1	-0.98	45.9
axial tension	3.8	3.3	3.7	3.8	3.7	4.3	3.8	3.3	2.9	3.3
rz shear	0.32	0.36	0.38	0.26	0.29	0.36	0.4	0.5	0.5	16.0
hoop strain	0.0024	0.0036	0.0051	0.0021	0.0033	0.0047	0.0032	0.0044	0.0057	2.5

Radial compression	45	ksi	Note: All strength and stress units are KSI
Axial tension	14	ksi	
rz shear	8	ksi*	
Hoop strain	1.40%	ksi	(from elevated temperature tests at 275 °F)

* from earlier database, needs to be verified

The CHPS flywheel topology provides an effective, high power density energy storage module capable of addressing the performance requirements of the PFN charging application. Tables 3 and 4 show the rotor design and machine envelope dimensions generated using the rotor design tool.

Table 3. Baseline CHPS sizing using TRV calculations.

MATLAB RESULTS

Rotor

	B/U Brg (x2)	Combo MB	Combo MB HSG	Radial MB	Radial MB HSG	Composite Rings	PM Back Iron*	PM Cartridge	PM Sleeve	Low Back Iron*	Top Back Iron*	Total
Mass (kg)	14.2	14.5	12.9	17.0	3.3	131.0	49.5	36.7	2.0	2.5	5.3	288.8
Jp (kg-m^2)	4.25E-01	0.31	0.39	0.48	0.11	6.56	1.61	1.00	0.05	0.09	0.19	11.21
Jt (kg-m^2)	2.46E+00	1.25	1.16	2.02	0.40	11.02	1.22	0.81	0.04	0.27	0.55	21.19
Stored Energy (MJ)	0.93	0.67	0.85	1.06	0.24	14.39	3.54	2.19	0.11	0.19	0.42	24.59

*Note: Rotating Back Iron is divided into PM Back Iron, Lower Back Iron and Upper Back Iron sections for computational purposes.

Stator and Miscellaneous Performance Results

Vac Hsg Mass	Vac Hsg OD	Vac Hsg OAL	Shaft Mass	MG Mass	Total Brg Mass	Stator Total Mass	ShearLimPwrMax(MJ)	ShearLimPwrMin(MJ)	Rotor CM	Jp/Jt	Min RPM	Discharge Depth	Del Energy (MJ)
97.2	0.550	0.986	84.1	52.1	71.2	304.6	11.5	8.5	0.427	0.53	14,859	26%	11.02

Housing OD (in) = 21.7 *Mass (kg) = 593* *Volume (liter) = 234*

Table 4. Optimized CHPS design with additional T1000G flywheel ring.

MATLAB RESULTS

Rotor

	B/U Brg (x2)	Combo MB	Combo MB HSG	Radial MB	Radial MB HSG	Composite Rings	PM Back Iron*	PM Cartridge	PM Sleeve	Low Back Iron*	Top Back Iron*	Total
Mass (kg)	14.2	14.5	12.9	17.0	3.3	192.6	49.5	36.7	2.0	2.5	5.3	350.4
Jp (kg-m^2)	4.25E-01	0.31	0.39	0.48	0.11	10.96	1.61	1.00	0.05	0.09	0.19	15.60
Jt (kg-m^2)	2.46E+00	1.26	1.17	2.00	0.39	16.86	1.22	0.81	0.04	0.26	0.55	27.03
Stored Energy (MJ)	0.93	0.67	0.85	1.06	0.24	24.03	3.54	2.19	0.11	0.19	0.42	34.22

*Note: Rotating Back Iron is divided into PM Back Iron, Lower Back Iron and Upper Back Iron sections for computational purposes.

Stator and Miscellaneous Performance Results

Vac Hsg Mass	Vac Hsg OD	Vac Hsg OAL	Shaft Mass	MG Mass	Total Brg Mass	Stator Total Mass	ShearLimPwrMax(MJ)	ShearLimPwrMin(MJ)	Rotor CM	Jp/Jt	Min RPM	Discharge Depth	Del Energy (MJ)
111.0	0.601	0.986	84.1	52.1	71.2	318.4	11.5	9.6	0.426	0.53	16,730	16%	10.28

Housing OD (in) = 23.7 *Mass (kg) = 669* *Volume (liter) = 280*

10 ALPS and MPM Program Review

The final task was to assess the potential for crossover technology from two earlier University of Texas programs: the Advanced Locomotive Propulsion System (ALPS) Program and the Megawatt Power Module for Ship Service Program. These both required modeling and simulation and the development of control algorithms for management of stored energy in isolated power systems using small gas turbine (~3 MW) prime movers. ALPS Program

The goal of the ALPS program was to demonstrate the feasibility of a hybrid electric propulsion system for a self-powered locomotive for 150 mph high speed passenger rail. Prime power for the locomotive was provided by a 3 MW gas turbine directly driving a high speed alternator. A 480 MJ energy storage flywheel was used to load level the gas turbine, recover braking energy, and provide supplemental power for acceleration and negotiation of grades. Figure 22 shows a simplified block diagram of the ALPS system; highlighted elements were developed and demonstrated during the program.

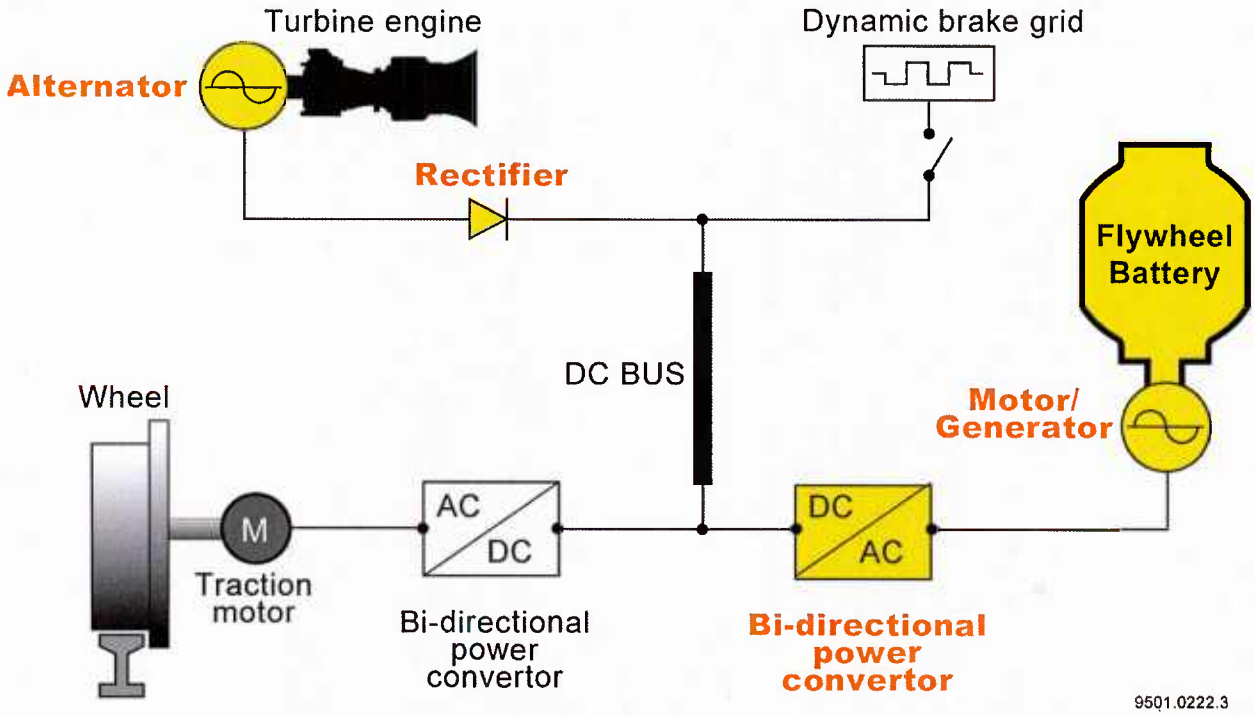

Fig. 22 ALPS system block diagram.

Two gas turbine prime movers were studied during the program, the Honeywell TF40 and the Pratt & Whitney ST-150. Both engines produce 3 MW at ISO conditions with a power turbine speed of 15,000 rpm. The engine was directly coupled to an 8-pole wound field synchronous generator developed in conjunction with AlliedSignal/ Honeywell. Output of the high speed alternator was converted to dc by a passive diode rectifier for powering the locomotives ~2,000 V_{dc} bus. The system also featured a 2 MW, 480 MJ energy storage flywheel which operated between 7,500 and 15,000 rpm. The flywheel included a 2 MW induction motor/generator to provide the electro-mechanical energy conversion. The flywheel was interfaced to the dc bus by a custom soft-switching power converter of the Auxiliary Resonant Commutated Pole (ARCP) topology.

A top level block diagram of the system controls is shown in Figure 23. The ALPS system was designed for integration with a locomotive supervisory controller and much of the overall energy management functionality was outside of the UT-CEM scope. The interface controller provided a link between the locomotive supervisory controller and the flywheel and gas turbine controllers. Unlike most power system applications, because train and detailed route information are known the demands on the power and energy storage systems can be defined a priori. This situation is further complicated by the requirement to replicate the existing 8-notch throttle control architecture typical to locomotives. This hybrid power system was successfully demonstrated in the UT-CEM laboratory.

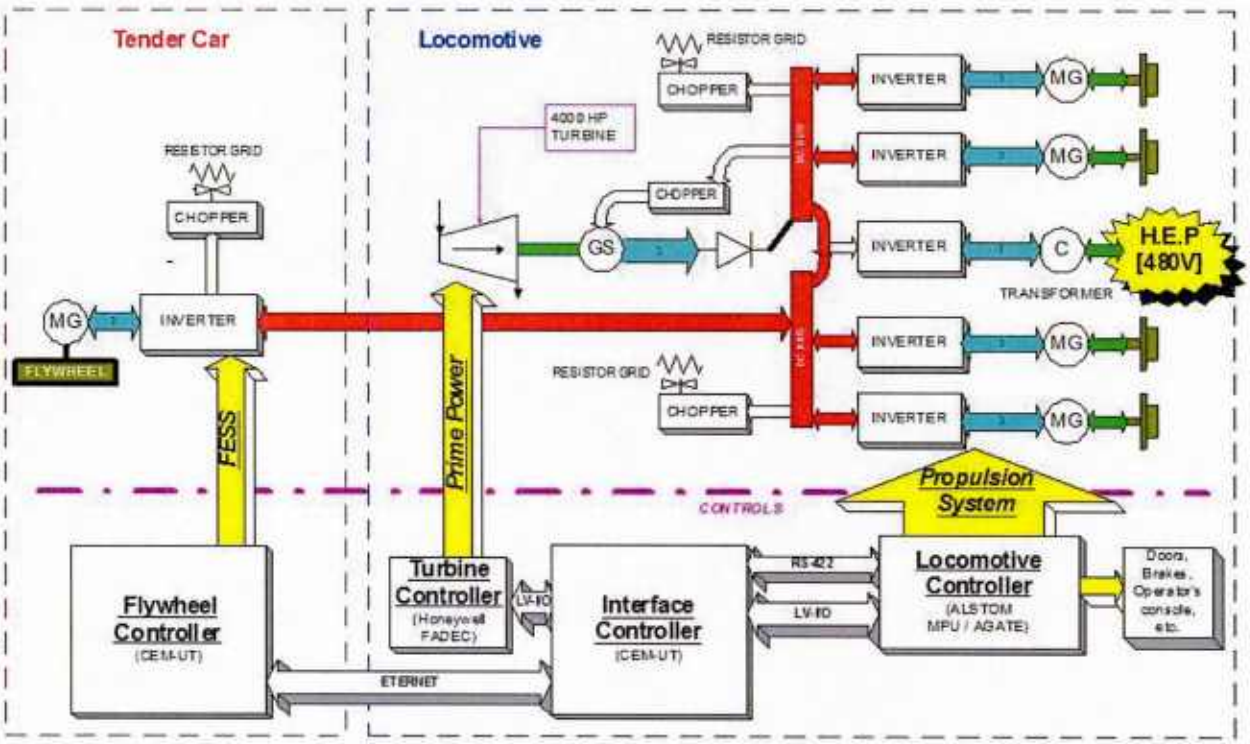

Fig. 23 ALPS control system block diagram.

10.1 Megawatt Power Module for Ship Service

The goal of the Megawatt Power Module (MPM) for Ship Service program was to explore the use of high speed generation and flywheel energy storage to improve the efficiency of the DDG51 ship service electric power distribution system by enabling operation with a single generator in non-threat environments. UT-CEM partnered with Rolls-Royce for this program

To enable backfit onto existing platforms, the new system fits in the same volume and footprint as the existing AG9140 turbine generator sets. Concept of operations (CONOPS) for the DDG51 calls for two ship service generators to be online at all times to prevent loss of power (dark ship) in the event of a failure of a single unit. Although it contributes to higher reliability, the poor part-load efficiency of gas turbines makes this mode of operation highly inefficient. Using direct drive high speed generators both increased power density and eliminated the gearbox which freed sufficient volume to incorporate multiple energy storage flywheels. The

energy store provides un-interruptible power (UPS) for a duration sufficient for multiple start attempts on a second "stand-by" turbine generator set. The system provides 2.5 MW for ten minutes. Operation on a single generator moved the typical DDG51 electric load closer to the engine's rated load, greatly improving specific fuel consumption. The improved performance of the twin shaft engine and elimination of the gearbox also contributed to efficiency. Figure 24 is a rendering of one variant explored during the program.

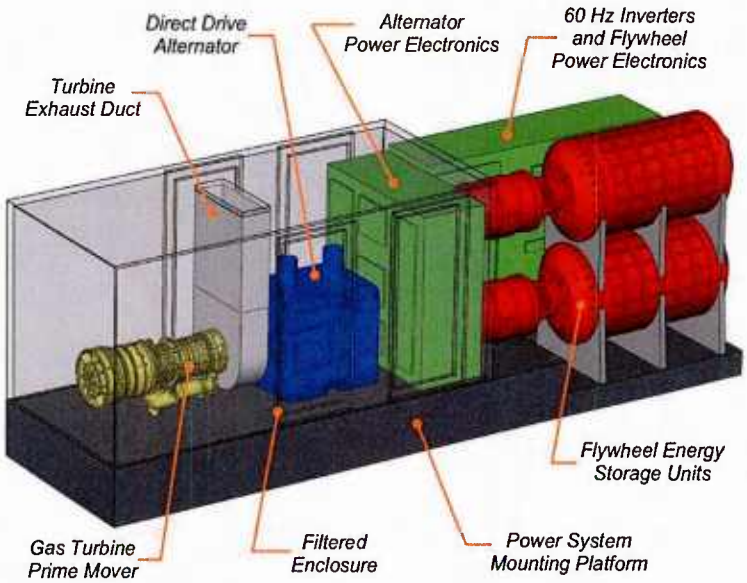

Fig. 24 General arrangement of one variant of the Megawatt Power Module.

.;

Figure 25 is a block diagram of the MPM system showing the baseline architecture; several variants were explored with a range of flywheel and motor/generator ratings.

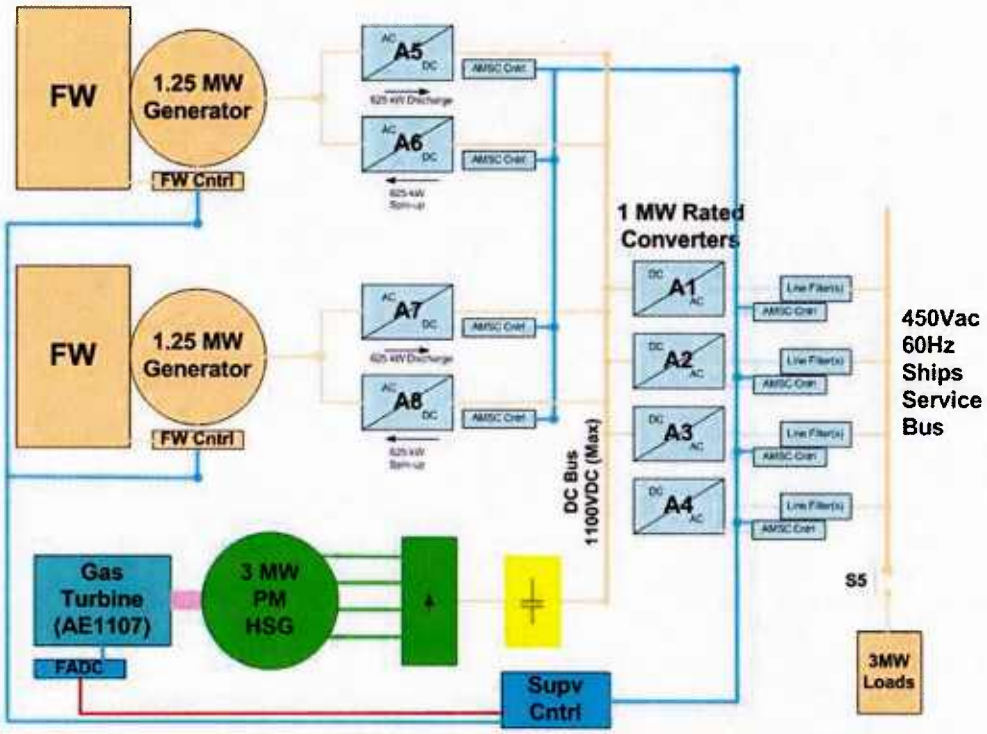

Fig. 25 Block diagram of the MPM system – two flywheels per skid configuration.

More extensive modeling and simulation was conducted for the MPM program including the development of preliminary control algorithms to manage the energy storage functions. Figure 26 is an overview of the MatLab Simulink model of the MPM system for a two flywheel configuration showing some of the major block functionality.

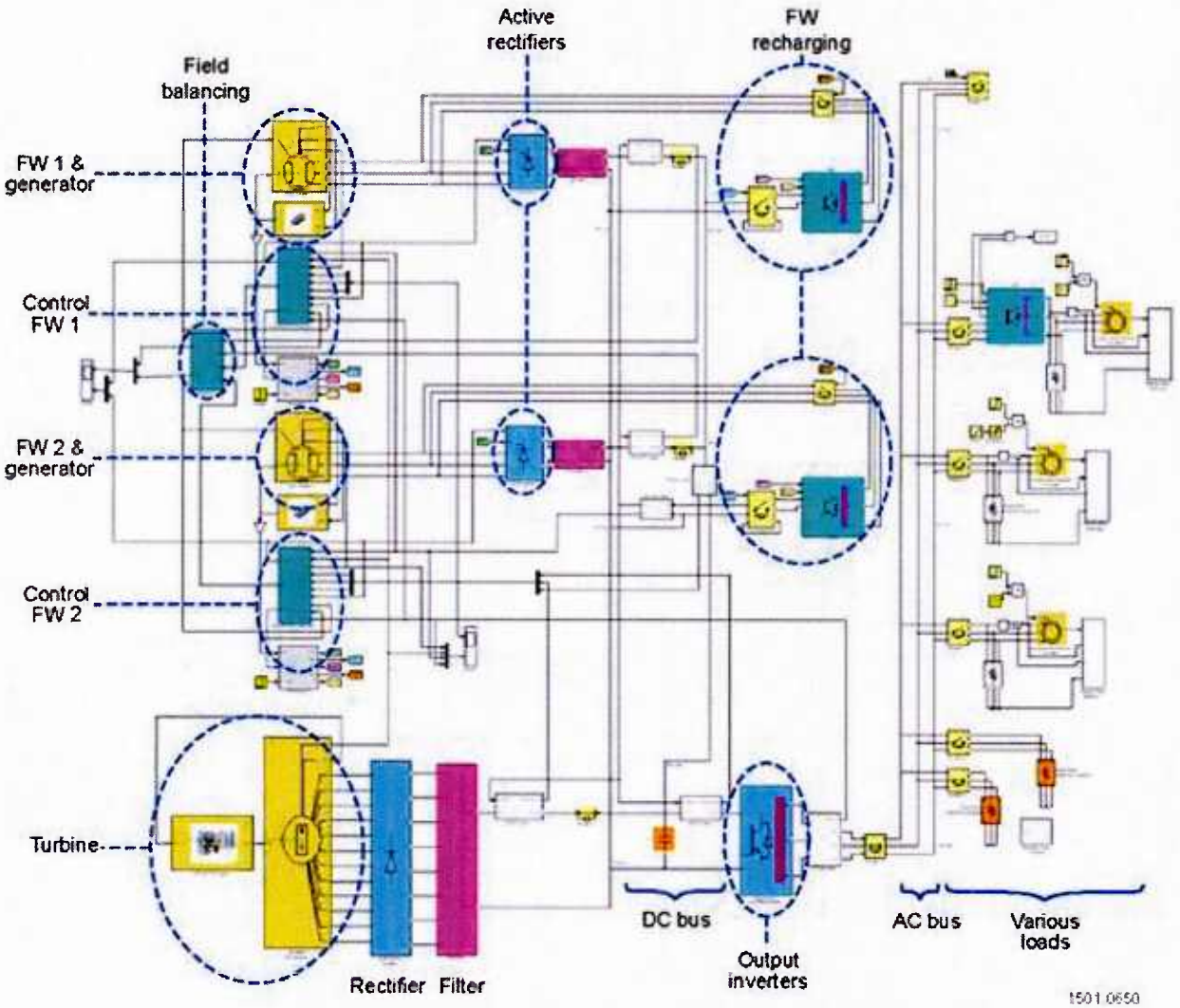

Fig. 26 MatLab Simulink model of a two-flywheel MPM configuration.

Of particular interest for the HESM program is the control algorithm used to manage the stored energy. Figure 27 is a top level flowchart of the control algorithm used in the MPM modeling.

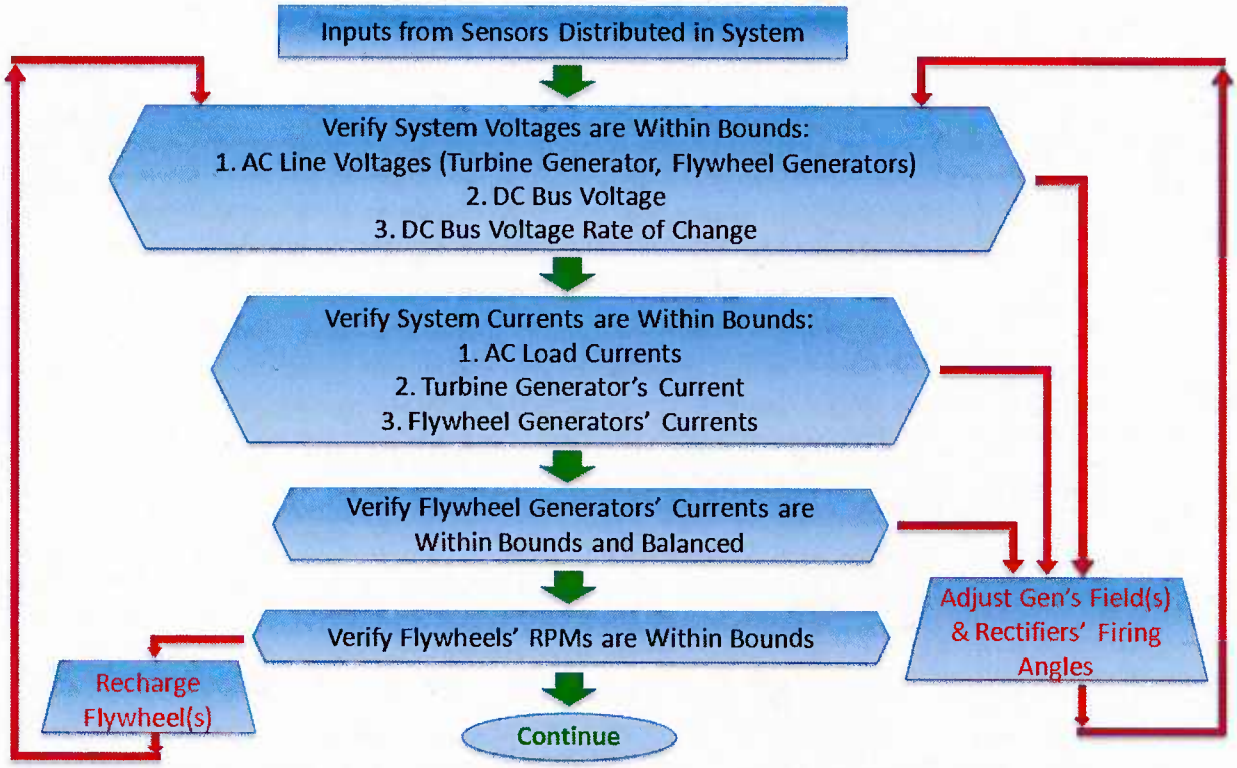

Fig. 27 Flowchart of the energy storage control methodology for the MPM program modeling.

11 Summary and Conclusions

The design and integration of a Hybrid Energy Storage Module (HESM) to mitigate the impact of transient (pulsed) loads on the ship's distribution power system has been studied. The pulsed load was assumed to be a high-energy capacitor-based Pulse Forming Network (PFN) operated with a repetition rate of 12 charge/discharge cycles per minute.

Two topologies for the HESM placement within the ship's power system were considered: centralized (single HESM and PFN) and distributed (multiple HESMs and PFNs). Furthermore, each topology was evaluated using two PFN charging profiles: constant current charging and hybrid charging. Each PFN charging profile was then simulated first using controlled ideal sources for the HESM and the PFN, and then using actual models for the power electronic converters generators and motors used within the HESM and the ship's power system.

The control of the HESM was accomplished by means of a derived voltage reference signal (6.4) that served two purposes: to control the power flow in and out of the HESM controller, and to maintain constant ship current. The simulation results validated this equation as a proper way to control the HESM's bi-directional converter.

Also, an amp-hour analysis suggested approximate values for I_{ship} in each charging variant, where this value remains constant during PFN and HESM charging and discharging. An improper selection for this value would result in flywheel speed drifts. These drifts were indeed observed in the flywheel speed simulation results and stem from neglecting the dc voltage ripple and unpredictability of the exact PFN peak charging current—the latter being a function of its terminal voltage. The drift can be eliminated by tracking flywheel speed and adjusting the value of I_{ship} in (6.4) or by using the frequency control of the power converter.

The charge and discharge power levels of the HESM unit(s) affect the size of the bi-directional converter. Although there are many common power conversion elements, the weight and volume of the power conversion equipment is potentially a strong discriminator between the various architectures and needs to be addressed consistently to ensure accurate comparisons. The ESRDC developed basic volumetric and gravimetric power densities for different types of power electronic conversion technologies (e.g. rectifier, inverter, dc-dc converter) to allow for a common and consistent sizing approach for the various power converters found in the different architectures presented herein. This approach should enable comparisons between the weight and volume of the power conversion equipment for different architectures. At this stage of the study, calculation of the weight and volume of the equipment is based on the power requirements without attempting to identify commercially available devices or scale up to the next typical rating.

The work presented in this report suggests the exclusion of the constant current charging profiles since its higher peak PFN charging power requirements impose stricter specifications on the PFN charging power supplies and HESM unit which reflect on the construction size and cost. The work showed that an architecture based on a HESM concept to minimize the impact of pulsed power loads on a ship's power system is feasible and very effective. Furthermore it confirms that the HESM can be used as an additional support element for the ship's power

system when not needed for pulsed load charging (e.g. UPS duty), thus making it a very versatile component for a variety of tasks.

References

[1] "Naval Ships' Technical Manual (Ch. 320) - Electrical Power Distribution Systems (rev. 2)," ed, 1998 [Online]. Available: http://www.hnsa.org/doc/nstm/ch320.pdf.

[2] IEEE Std 45-1998, *Recommended Practice for Electric Installation on Shipboard.*

[3] IEEE Std 1709-2010, *Recommended Practice for 1 kV to 35 kV Medium-Voltage DC Power Systems on Ships.*

[4] IEEE Std 315-1975 (Reaffirmed 1993), *Graphic Symbols for Electrical and Electronics Diagrams.*

[5] National Fire Protection Association, *NFPA 70 - National Electric Code*, 2005.

[6] DoD Military Handbook MIL-HDBK-299 (SH) (1989), *Cable Comparison Handbook - Data Pertaining to Electric Shipboard Cable.*

[7] DoD Military Specification MIL-C-24643A (1994), *Cables and Cords, Electric, Low Smoke, For Shipboard Use, General Specification for.*

[8] Southwire Company, *Power Cable Manual*, 4th ed., 2005.

[9] S. B. Pratap, "EMALS Analysis Report: Energy Storage System – Shipboard," submitted to General Atomics, 2004.

[10] A. M. Trzynadlowski, *Introduction to Modern Power Electronics*: Wiley, 2010.

[11] W. Jiang, "Load sharing techniques in hybrid power systems for dc micro-grids," in *Power and Energy Engineering Conference (APPEEC),*, 2011, pp. 1-4.

[12] V. J. Thottuvelil, "Stability analysis of parallel DC/DC converters with active current sharing," in *Power Electronics Specialists Conference*, 1996, pp. 1080-1086.

[13] A. Ouroua and S. Santoso, "Integration of high-frequency components in MW-level power systems with alternative secondary distribution networks," in *Electric Ship Technologies Symposium*, Alexandria, VA, April 10-13, 2013.

[14] T. J. E. Miller, *Brushless Permanent Magnet and Reluctance Motor Drives*: Oxford University Press, 1993.

12 APPENDIX 1. HESM Simulink Models

The following three items listed in this Appendix have been delivered to Tracy Hannon of NAVSEA on May 1, 2013.

Input Data File HESMm_PFN1_R1

HESMm_PFN1_R1.m

```
% SHIP WITH HYBRID ENERGY STORAGE MODULES
% Created by The Center for Electromechanics of The University of Texas for
% The Office of Naval Research and The Naval Surface Warfare Center
% April 30, 2013
%
% Input items needed for the simulation of a Ship Power System with a
% number m of Hybrid Energy Storage Modules and a single Pulse Forming
% Network.
%
% NOTE: make sure to enter all required parameters, either directly or via
%       input menus, in all blocks or elements with colored background
%       (not white) at ALL levels (remember to "Look Under Mask").
%       In general, items below the top level need to be changed only
%       rarely for a given design.
%
Ts=0.000005;      % Simulation step time, seconds
Tend=20;          % Simulation end time, seconds
%
Nh=4;             % Number m of HESMs
Ng=2;             % Number of ship generators
%
Iship0=2762;      % Estimated constant current from ship's power system
Rh=0.1;           % HESM cable resistance, Ohms
%
% Flywheel data for single or multiple HESM: used in each HESMm block
%                 (read block's input menu) and in yellow blocks within the
%                 "Measurement" block (white background).
%
%                 Note: Enter actual values of FJm and w0m for each HESMm.
%
%                 Note: Match the variable subscript to the subscript of
%                       the HESM block actually used: e.g., FJ1 and w01
%                       will provide inputs for HESM1, likewise FJ2 and w02
%                       for HESM2, etc.
%
```

```
36      %                 Note: 4 HESM blocks have been provided with the original
37      %                       model. If Nh>4 new HESM blocks must be generated
38      %                       copying them from the other HESM blocks and making
39      %                       the appropriate changes internal to the new blocks
40      %                       (Read the block's input menu). Also add additional
41      %                       lines herein for the FJm and w0m values needed.
42      %                       "Measurement" block also may be updated accordingly
43      %                       if desired.
44      %
45 -    FJ1=1128/Nh;       % Flywheel 1 Inertia, kg*m^2
46 -    w01=3600;         % Flywheel 1 initial speed, RPM
47 -    FJ2=1128/Nh;       % Flywheel 2 Inertia, kg*m^2
48 -    w02=3600;         % Flywheel 2 initial speed, RPM
49 -    FJ3=1128/Nh;       % Flywheel 3 Inertia, kg*m^2
50 -    w03=3600;         % Flywheel 3 initial speed, RPM
51 -    FJ4=1128/Nh;       % Flywheel 4 Inertia, kg*m^2
52 -    w04=3600;         % Flywheel 4 initial speed, RPM
53      %
54      % PFN charging cycle: enter a sequence of 5 monotonically increasing times
55      %                             t0  <  t1  <  t2  <  t3  <  t4
56      %                   with corresponding 5 values of required PFN powers
57      %                            P0     P1     P2     P3     P4
58      %                   Within each time interval the power curve will be
59      %                   generated by linear interpolation, e.g.
60      %                      if t1<t<t2 then P(t) = P1+(P2-P1)/(t2-t1)*(t-t1)
61      %                   If fewer than 5 point pairs are sufficient simply repeat
62      %                   the last pair identical to itself as needed: e.g. if
63      %                   only four pairs are sufficient make t4=t3 and P4=P3.
64      %                   Cycle repeats up to Tend. Note: make Plast=P0.
65 -    t0=0;        P0=0;
66 -    t1=1;        P1=23;
67 -    t2=4;        P2=23;
68 -    t3=4.25;     P3=0;
69 -    t4=5;        P4=P0;
70      %
71      %                END
72
```

Model HESM4_PFN1_R1

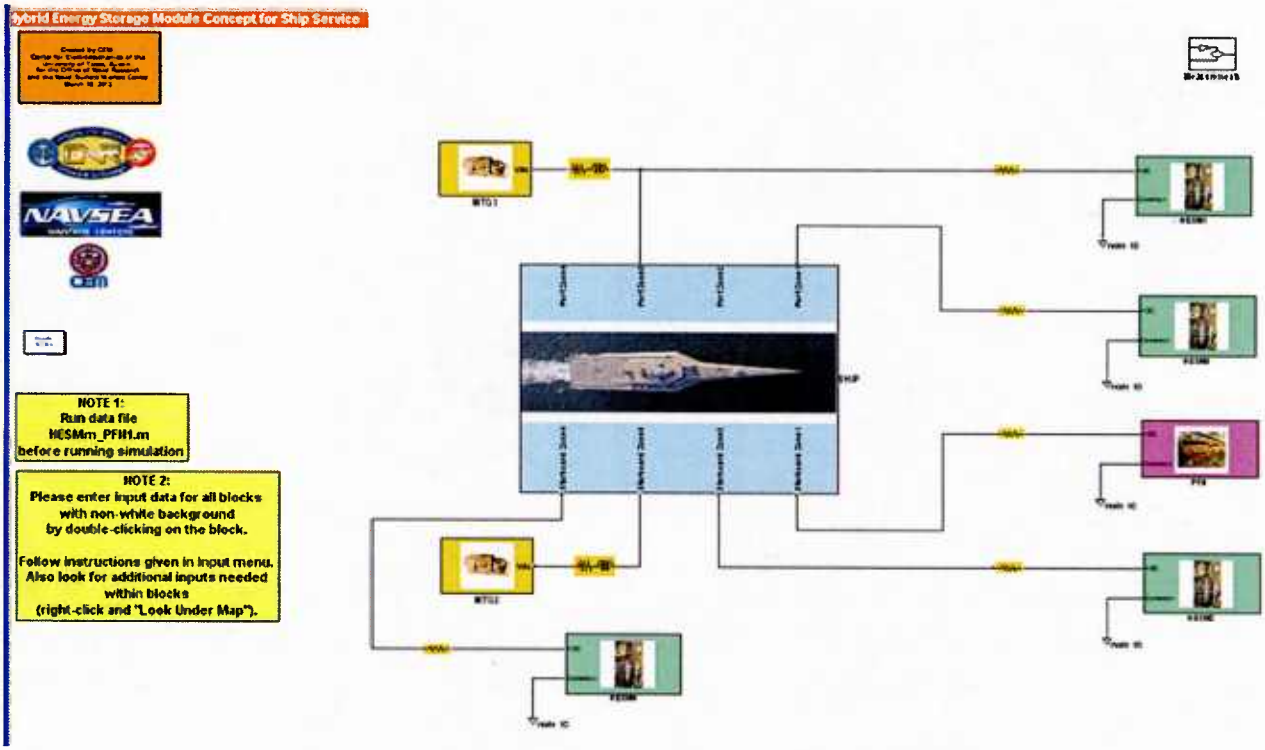

Model HESM2_PFN1_R1